18. Solar Atmosphere

Solar Atmosphere

- Structure of the Solar Atmosphere
- Models of the Solar Atmosphere
- Filaments and Prominences
- Chromospheric Structures
- Spicules

Structure of the Solar Atmosphere

The solar atmosphere is a combination of the photosphere and the chromosphere. Sometimes, the solar corona is considered as an upper part of the atmosphere.

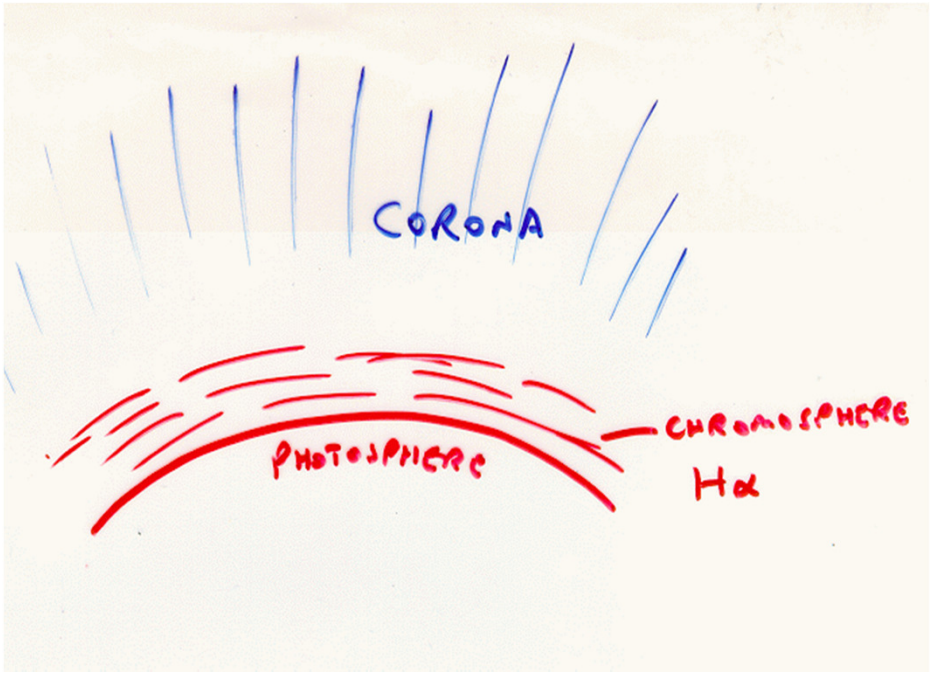

The **photosphere** is a layer of about 400 km thick where the solar gas changes from almost completely opaque to almost completely transparent. Most visible light originates in the photosphere. Thus, the photosphere may be thought of as the imaginary surface from which the solar light that we see appears to be emitted. The diameter quoted for the Sun usually refers to the diameter of the photosphere.

The transition from optically thin to optically thick depends on position on the Sun, and on wavelength, particularly, in the spectral lines. This allows us to study the thermodynamic properties of the solar atmosphere, its chemical composition and dynamics.

Solar Photosphere as a Function of Depth

Depth (km)	% Light from this Depth	Temperature (K)	Pressure (bars)
0	99.5	4465	6.8×10^{-3}
100	97	4780	1.7×10^{-2}
200	89	5180	3.9×10^{-2}
250	80	5455	5.8×10^{-2}
300	64	5840	8.3×10^{-2}
350	37	6420	1.2×10^{-1}
375	18	6910	1.4×10^{-1}
400	4	7610	1.6×10^{-1}

Some properties of the photosphere. This table indicates that the solar atmosphere changes from being almost completely transparent to being almost opaque over a distance of about 400 km. Notice also that in this region the temperature drops rapidly as we near the surface.

In a number of strong spectral lines the transition to optically thick state occurs high in the atmosphere. When we observe the Sun in such lines we see the upper part of the atmosphere called **the chromosphere**. This layer was named from its colorful appearance during solar eclipses.

The chromosphere is 2000-3000 km thick. It glows faintly relative to the photosphere and can only be seen easily in a total solar eclipse. When it can be seen it is reddish in color (because of strong Balmer H-alpha emission). This color is the origin of its name (*chromos* meaning ``color'').

The faint flow of the chromosphere is due to an emission spectrum from hot, low density gases emitting at discrete wavelengths. The discovery of helium noted earlier was from emission lines seen in the chromosphere during an eclipse in 1868. This new element was only found on the Earth in 1895.

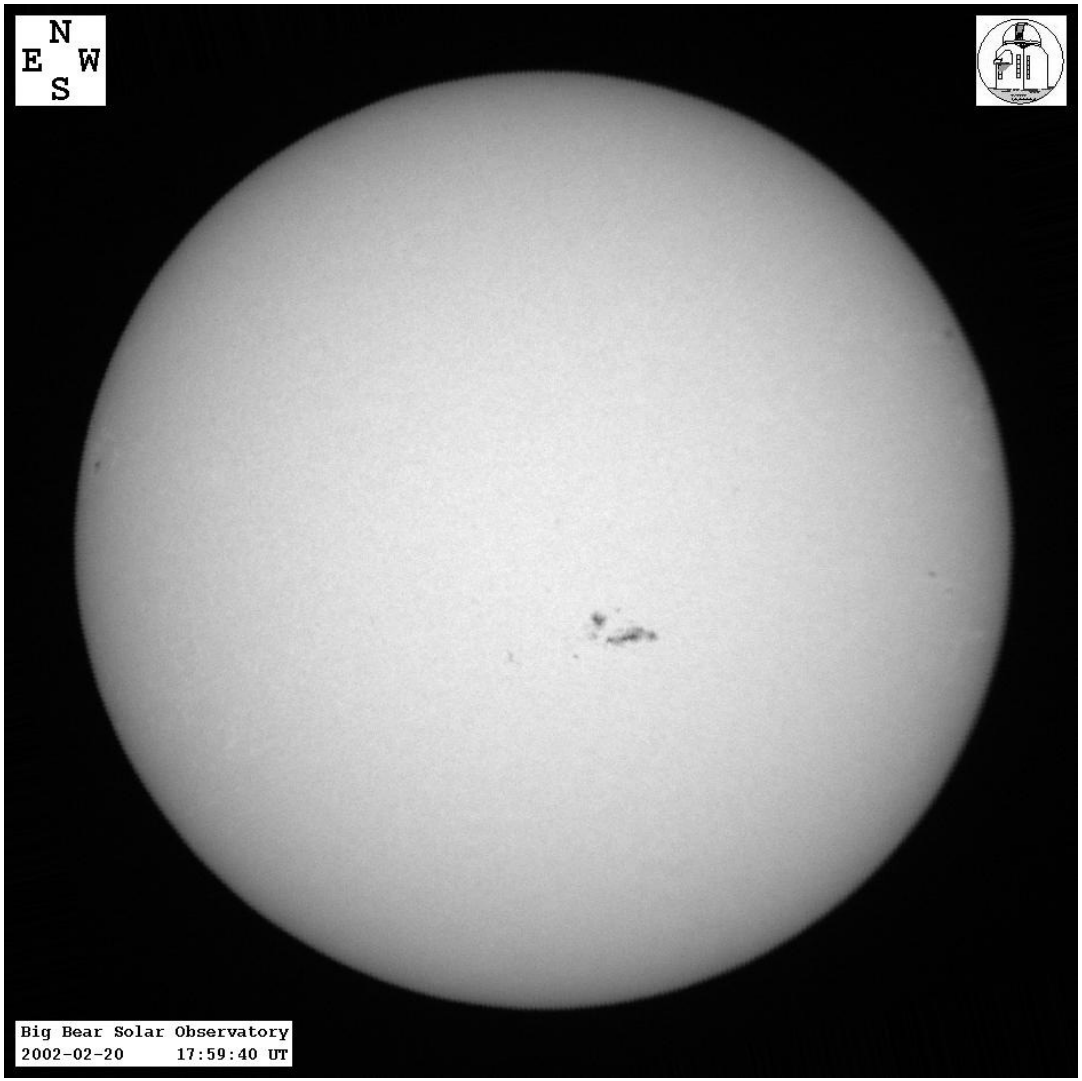

White-light image of the solar photosphere from Big Bear Solar Observatory, 2002-02-20, 17:59:40 UT. The image is darker near near the limb because there we see higher layers of the photosphere that are cooler.

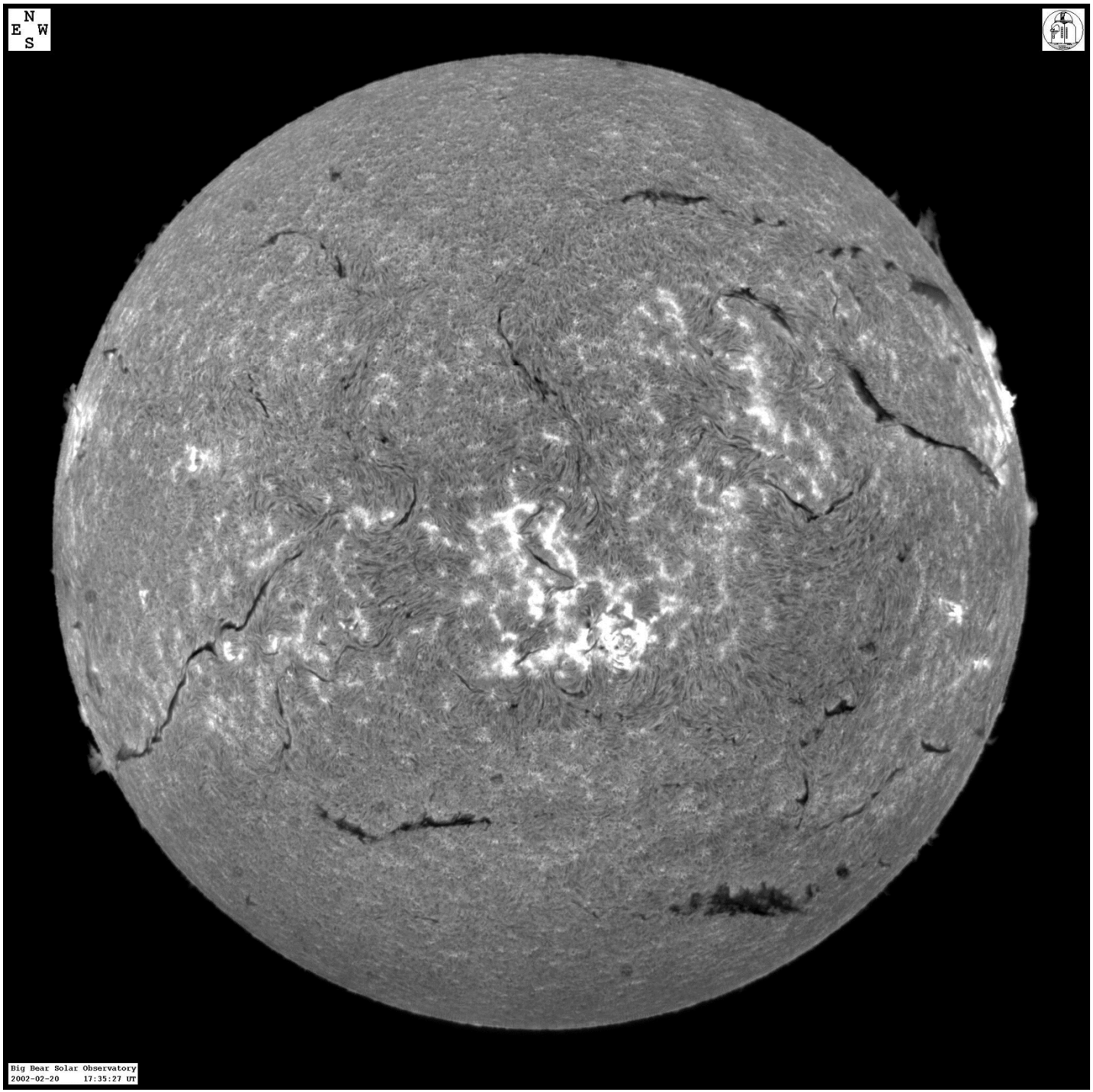

Image of the solar chromosphere in hydrogen H-alpha line from Big Bear Solar Observatory, 2002-02-20, 17:35:27 UT. This image shows dark (cool) filament and prominencies. Plasma temperature about 10,000 K.

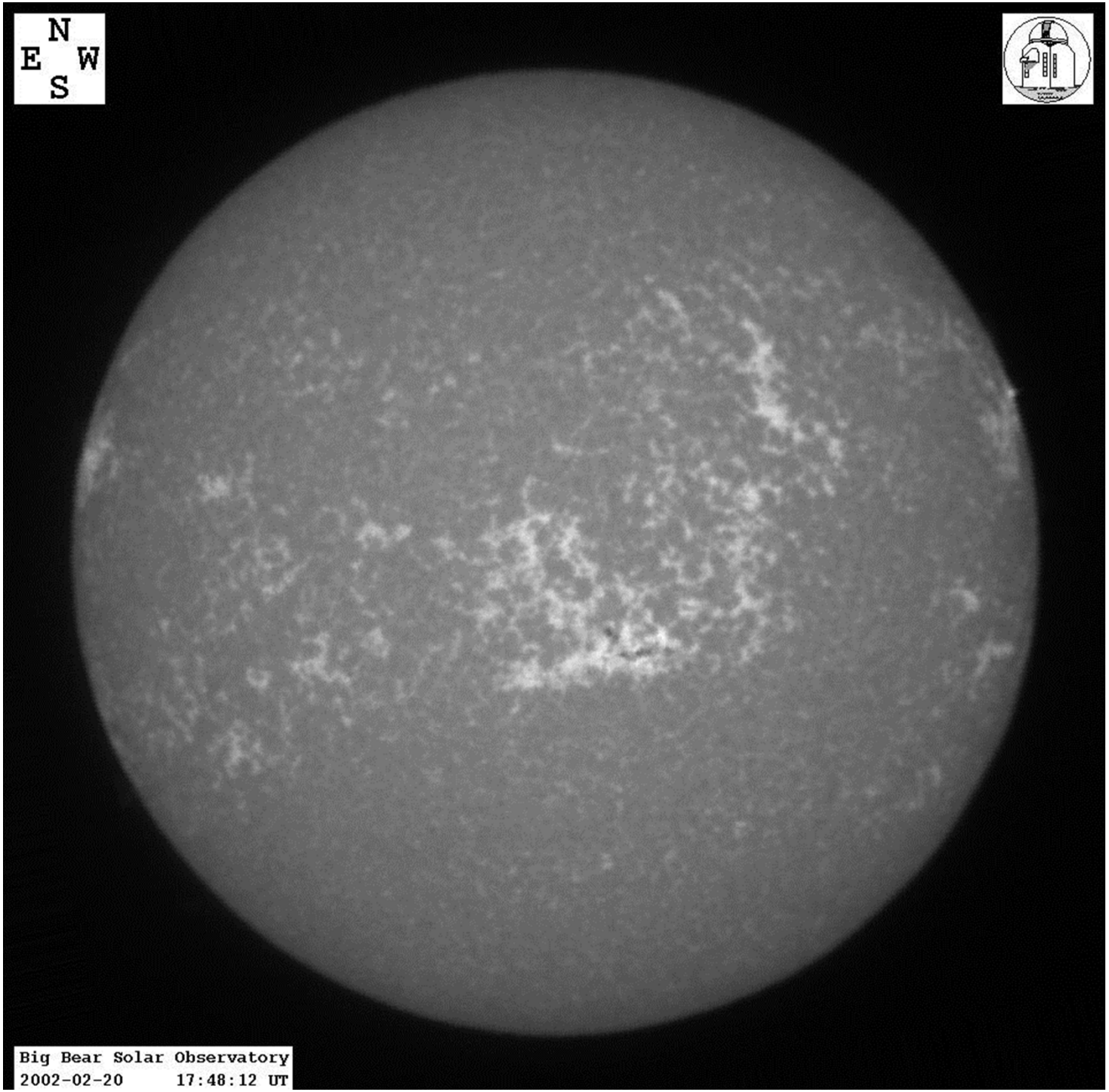

Image of the solar chromosphere in Ca K line from Big Bear Solar Observatory, 2002-02-20, 17:35:27 UT

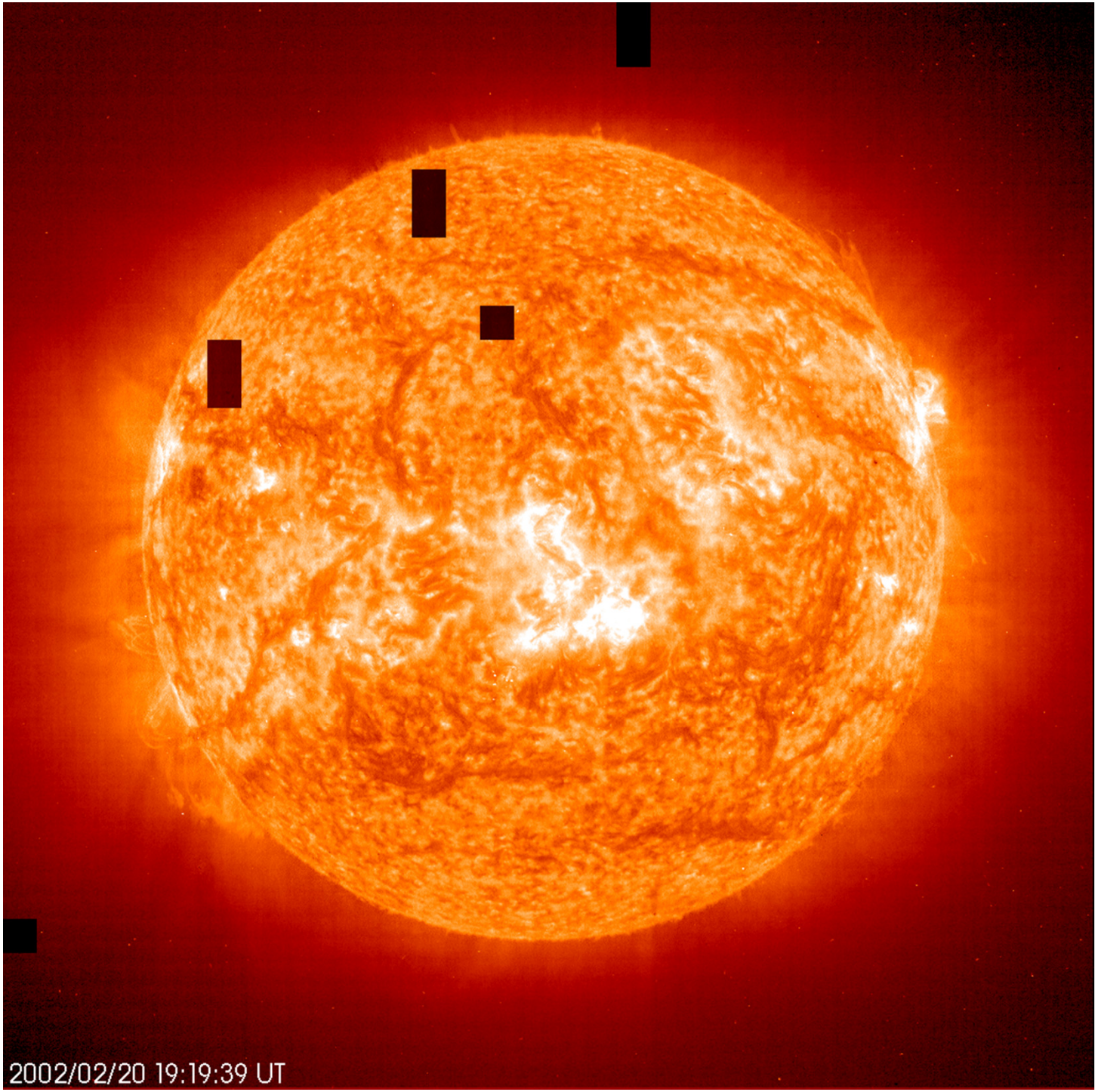

Image of the upper solar chromosphere in HeII, 304Å, line from SOHO EIT, 2002-02-20, 19:19:39 UT. It shows the solar plasma with $T \simeq 30{,}000\,\mathrm{K}$.

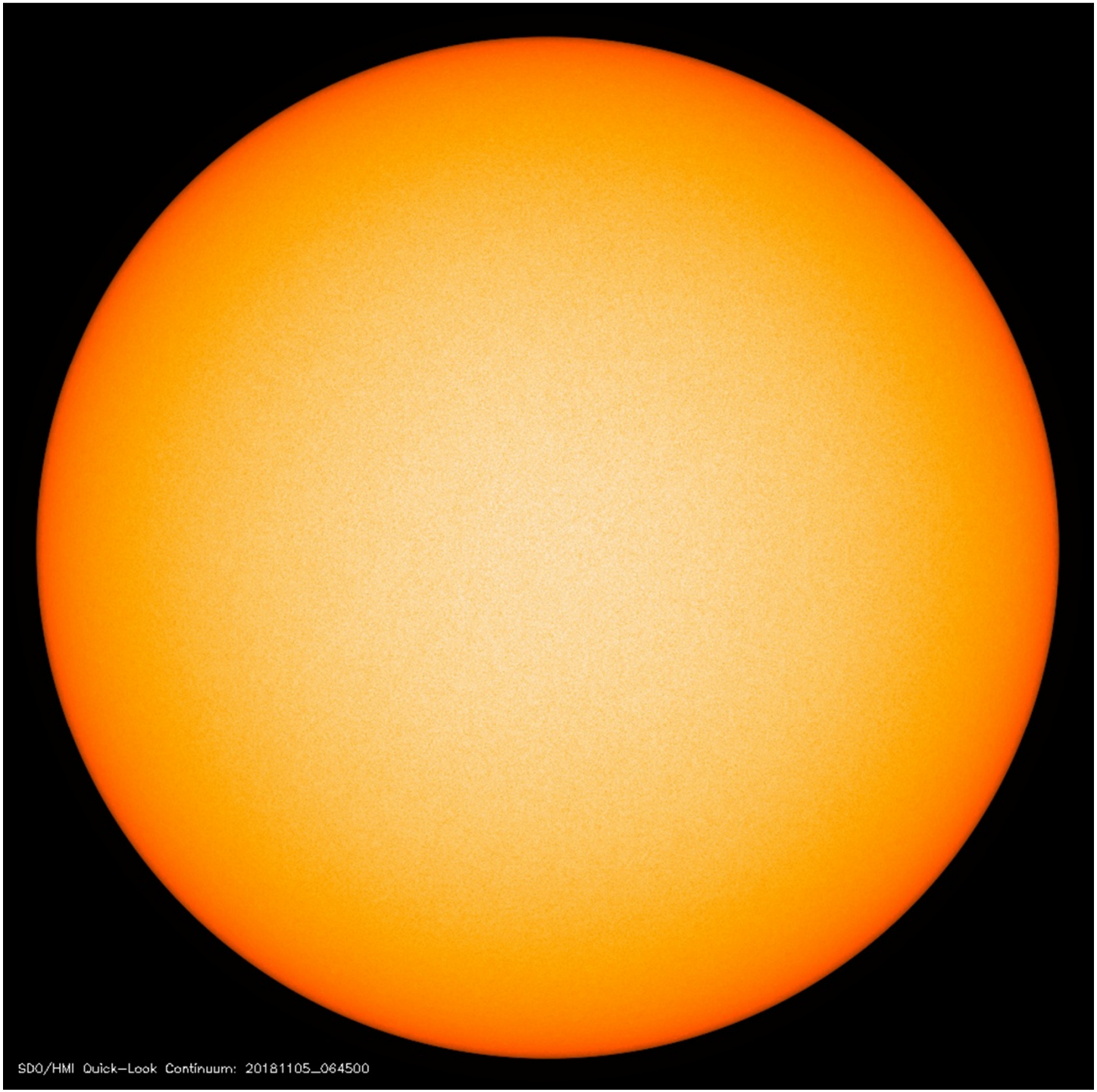

Today's image from the HMI instrument (Helioseismic and Magnetic Imager) on SDO.

Notice the limb darkening.

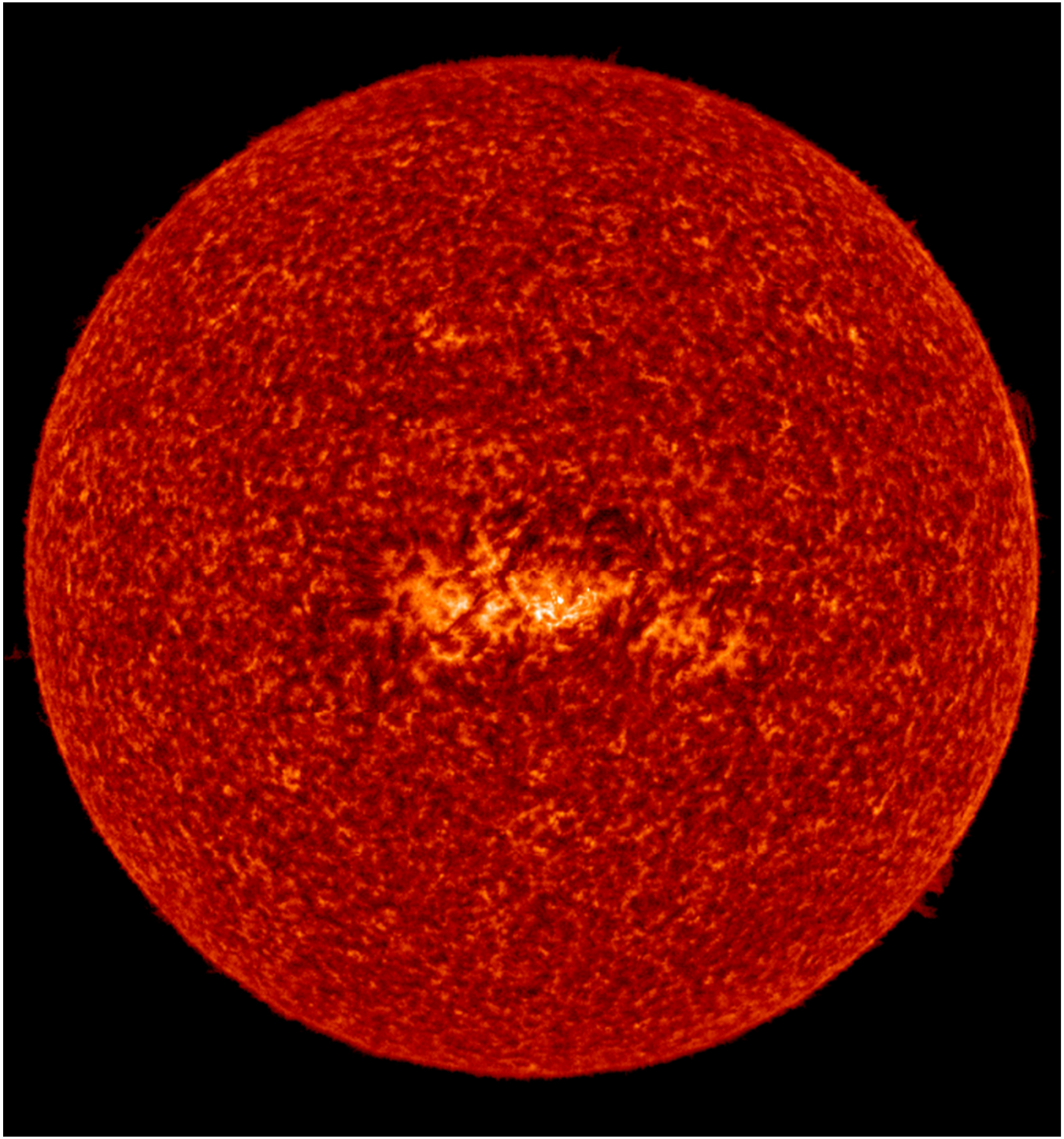

Full disk of the Sun on 12 May 1996, observed by SUMER instrument on SOHO alternating in H I Lyε (937 Å), S VI (933 Å), and S VI (944 Å) blended with Si VIII. An isolated active region can be seen near the center of the disk. Note the changing length of the plasma structures with the formation temperature of the emission lines and the absence of any significant limb brightening of the H I line, which is emitted from optically thick plasmas.

Notice that the limb is brighter in UV.

VIS: H-alpha Observations

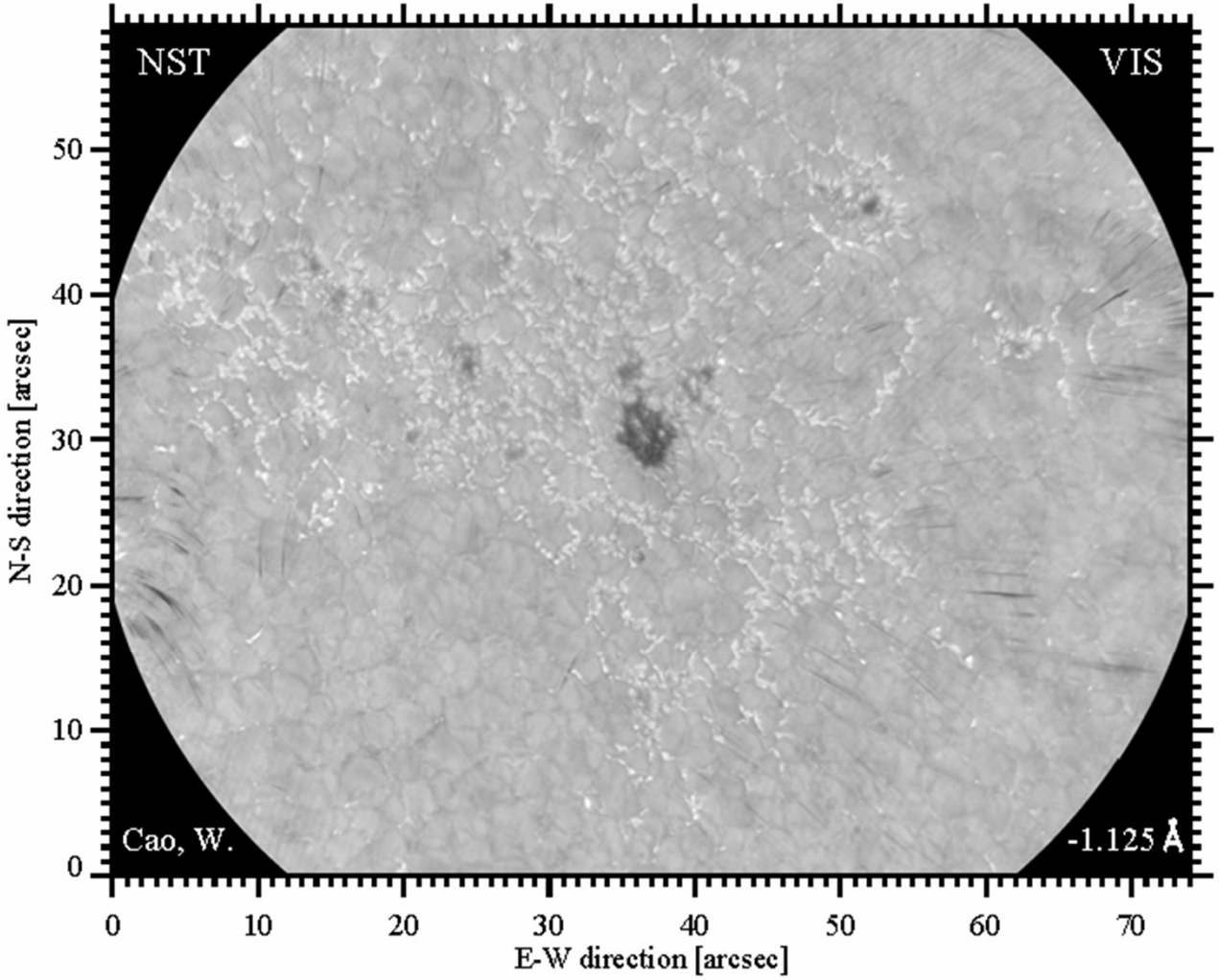

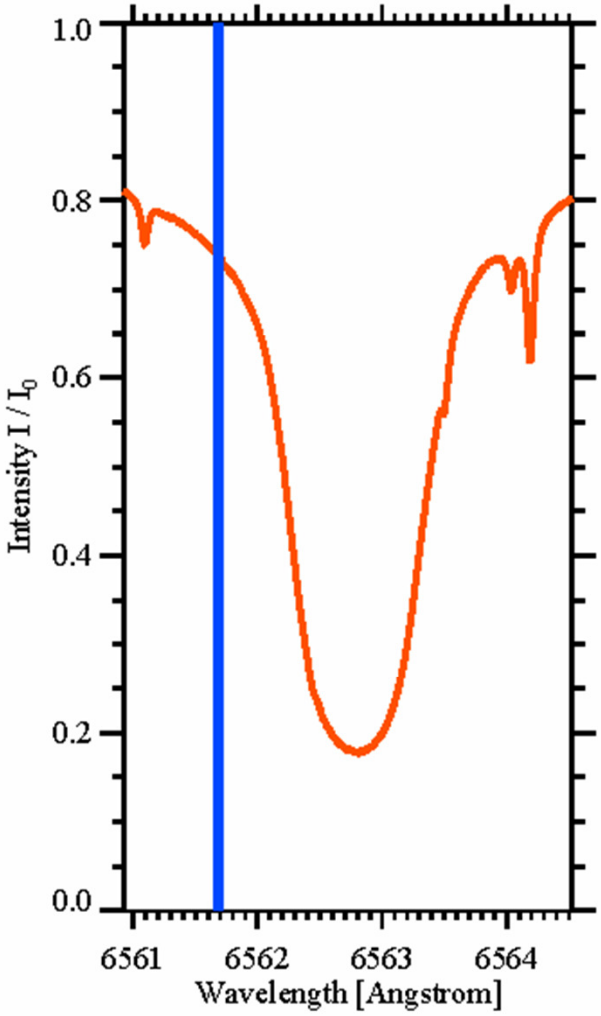

(Courtesy of W.Cao)

Temperature structure of the solar atmosphere

- To determine the temperature structure we need to consider the equation of radiative transfer and identify the sources of radiation absorption and emission.

2. Radiative Energy Transfer

Energy inside a star is transported by radiation and convection. Consider the radiative transport:

$$dI_\nu(\theta) = -\kappa'_\nu I_\nu(\theta) ds + \varepsilon_\nu ds,$$

where I_ν is the radiation intensity at frequency ν in direction θ, κ'_ν is the absorption coefficient per cm of the light path, ε_ν is the emission coefficient, $ds = dz / \cos\theta$. Then,

$$\cos\theta \frac{dI_\nu}{dz} = -\kappa'_\nu I_\nu(\theta) + \varepsilon_\nu = -\kappa'_\nu \left(I_\nu - \frac{\varepsilon_\nu}{\kappa'_\nu} \right).$$

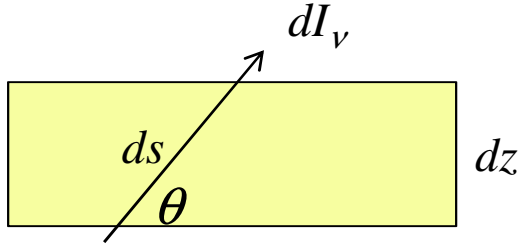

The ratio $\varepsilon_\nu / \kappa'_\nu$ is called the source function, S_ν.

Using the absorption coefficient per unit mass: $\kappa_\nu = \kappa'_\nu / \rho$, we obtain:

$$\frac{\cos\theta}{\rho\kappa_\nu} \frac{dI_\nu}{dz} = -\left(I_\nu - S_\nu \right).$$

Introducing optical depth: $d\tau_\nu = -\rho\kappa_\nu dz$ and defining $\mu = \cos\theta$ we get:

$$\mu \frac{dI_\nu}{d\tau_\nu} = (I_\nu - S_\nu).$$

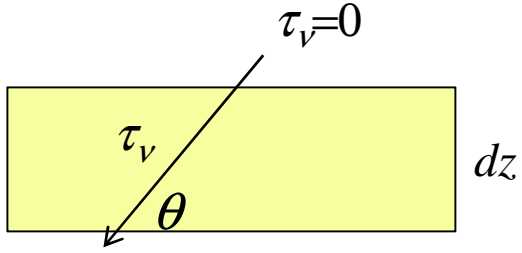

Models of the Solar Atmosphere

The models of the solar atmosphere describe how temperature, pressure and density change with the height.

Consider the equation of radiative transfer that describes how radiation intensity $I_\nu(\theta, z)$ at frequency ν changes with height z and propagation angle θ:

$$\mu \frac{dI_\nu}{d\tau_\nu} = I_\nu - S_\nu, \quad (1)$$

where $\mu = \cos\theta$, τ_ν is the optical depth

$$d\tau_\nu = -\kappa_\nu \rho dz,$$

κ_ν is the absorption coefficient per unit mass, S_ν is the source function (the ratio of emission and absorption coefficients, $\varepsilon_\nu / \kappa_\nu$.

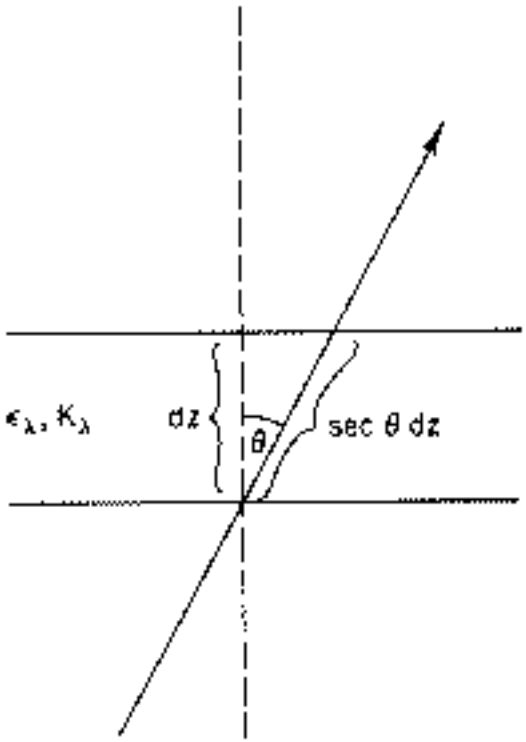

The radiative transfer equation (Eq.1) can be easily solved the integrating factor method.

The Eddington-Barbier relation

Integrating this equation from optical depth $\tau_1 = 0$ to $\tau_2 = \infty$ we get

$$I_\nu(0,\mu) = \frac{1}{\mu}\int_0^\infty S_\nu(\tau_\nu) e^{-\frac{\tau_\nu}{\mu}} d\tau_\nu,$$

the intensity emerging from the Sun at angle θ.

Consider a simple linear approximation to the source function: $S_\nu(\tau_\nu) = S_\nu(0) + b\tau_\nu$, where b is a constant.

Then,
$$I_\nu(0,\mu) = \int_0^\infty \frac{1}{\mu} S_\nu(0) e^{-\frac{\tau_\nu}{\mu}} d\tau_\nu + b\int_0^\infty \frac{1}{\mu}\tau_\nu e^{-\frac{\tau_\nu}{\mu}} d\tau_\nu.$$

$$I_\nu(0,\mu) = S_\nu(0) + b\mu.$$

Comparing this equation with the equation for $S_\nu(\tau_\nu)$ we see that the emergent intensity observed at angle θ if equal to the source function at the optical depth $\tau_\nu = \mu$.

That is $I_\nu(0,\mu) = S_\nu(\tau_\nu)$ at $\tau_\nu = \mu$.

This result known as the Eddington-Barbier relation, implies that if $S_\nu(\tau_\nu)$ is a linear function, the emergent monochromatic radiation viewed at angle μ can be interpreted to be formed at a surface whose depth is given by $\tau_\nu = \mu$.

Illustration of the varying depth of penetration into the solar photosphere implied by the Eddington-Barbier relation:

the emergent monochromatic radiation viewed at angle μ can be interpreted to be formed at a surface whose depth is given by $\tau_\nu = \mu$. This means that when we observed closer to the limb we see higher layers of the atmosphere.

$$I_\nu(0,\mu) = S_\nu(\tau_\nu) \quad \text{at } \tau_\nu = \mu.$$

This Eddington-Barbier relation implies that if $S_\nu(\tau_\nu)$ is a linear function, the emergent monochromatic radiation viewed at angle μ can be interpreted to be formed at a surface whose depth is given by $\tau_\nu = \mu$.

Using this relation we can determine how the optical depth varies with temperature in the atmosphere:

$\frac{d\tau_\nu}{dT} = \frac{d\mu}{dT} = \left(\frac{dT}{d\mu}\right)^{-1}$ if we measure how the radiation temperature changes with across the limb .

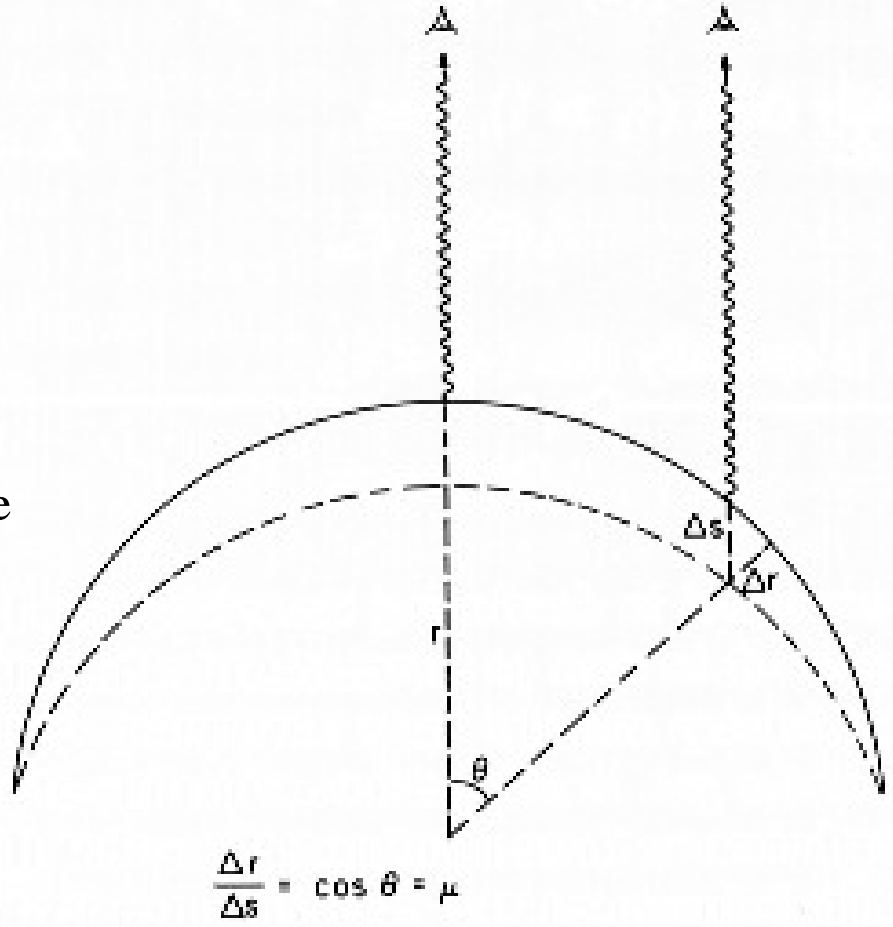

Determination of the absorption coefficient

For local thermodynamic equilibrium (LTE) conditions:

$$S_\nu(\tau_\nu) = B_\nu(T),$$

where $B_\nu(T)$ is the Planck function. If the condition are somewhat different from LTE we use the same relation but for an effective (bolometric) temperature T_b:

$$S_\nu(\tau_\nu) = B_\nu(T_b).$$

Then, the Eddington-Barbier relation is:

$$I_\nu(0,\mu) = B_\nu(T_b).$$

Using this relation we can determine $T_b(\mu)$ as a function of μ for observations of $I_\nu(0,\mu)$.

Consider now the definition of the optical depth:

$$d\tau_\nu = -\kappa_\nu \rho dz.$$

Differentiate this with respect to temperature T:

$$\frac{d\tau_\nu}{dT} = -\kappa_\nu \rho(z) \frac{dz}{dT}.$$

Here we assumed that κ_ν is the same in the photosphere for a given ν.

The left-hand side can determined directly from observation using the Eddington-Barbier relation we have:

$$\frac{d\tau_\nu}{dT} = \left(\frac{dT_b}{d\mu} \right)^{-1}.$$

Thus, we can determine the dependence of the absorption coefficient on frequency ν or wavelength λ.

Negative ions of hydrogen are the main source of photospheric absorption and emission.

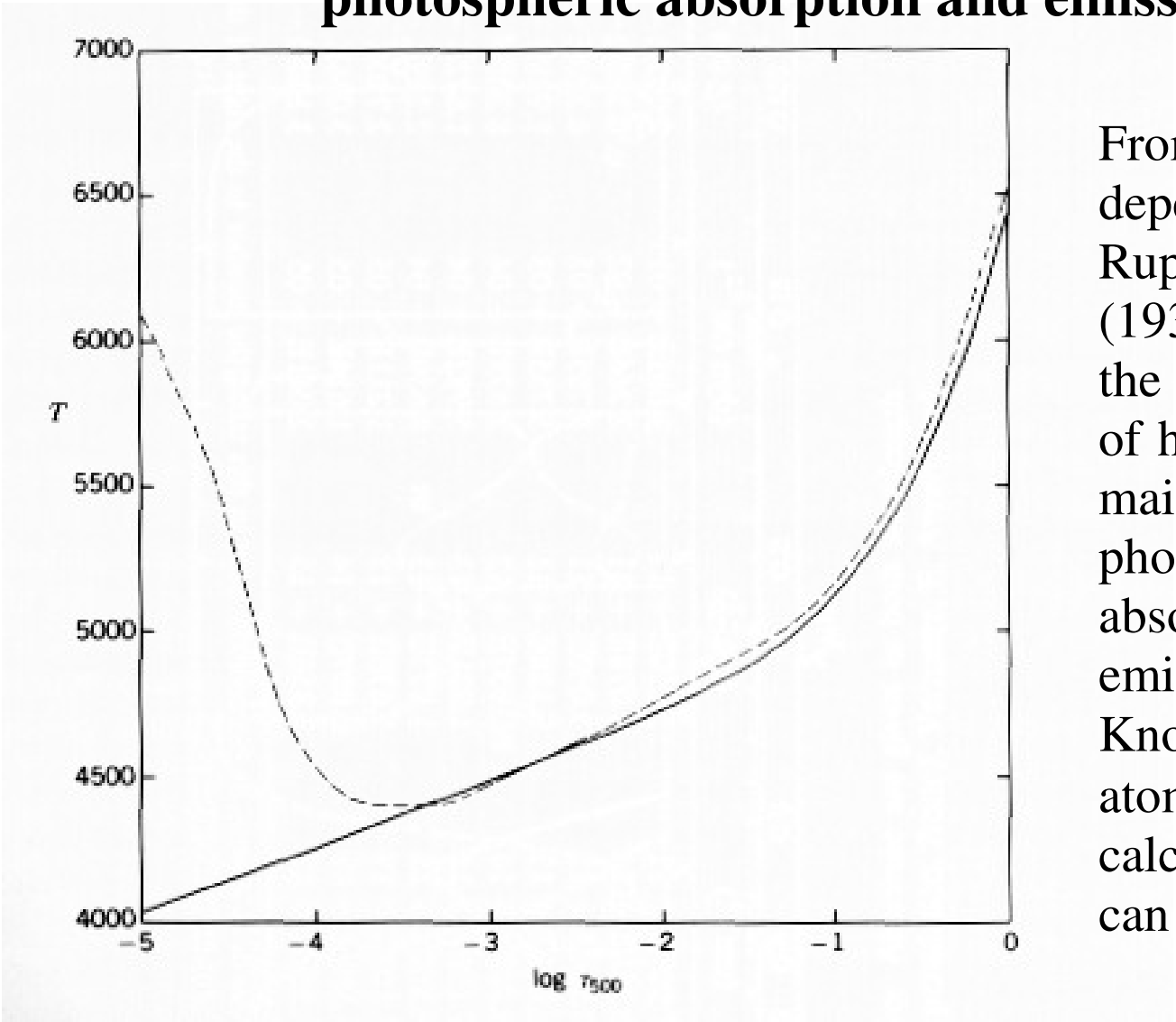

From these dependences Rupert and Wildt (1938) identified the negative ions of hydrogen as the main source of photospheric absorption and emission. Knowing κ_ν from atomic physics calculations we can determine $T(z)$

The photospheric temperature profile from the atmospheric empirical model (dashed curved), and a theoretical radiative-convective model (solid curve).

Illustration of the negative hydrogen ion

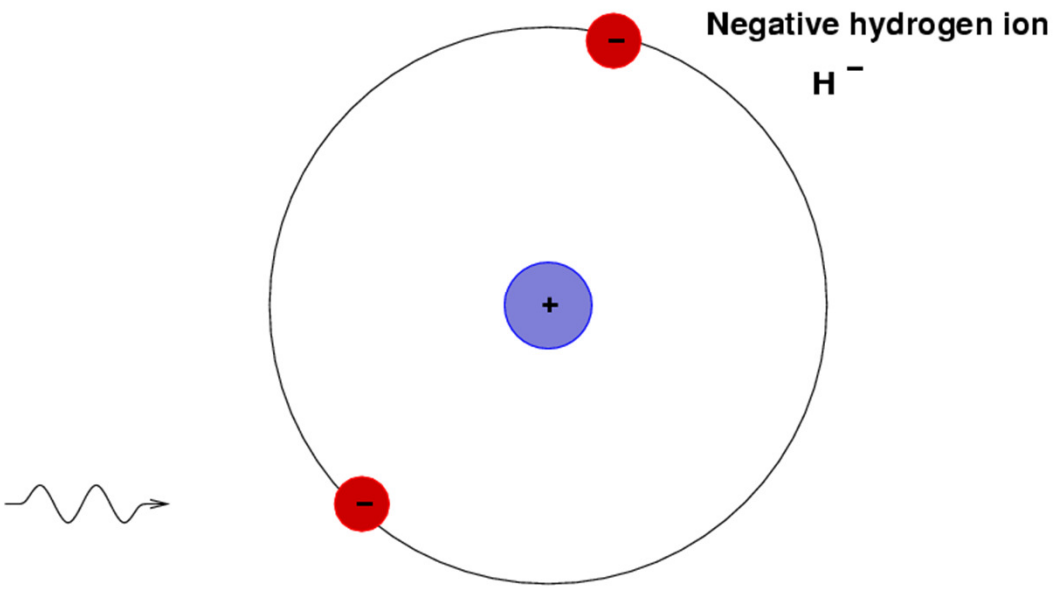

Photons are easily absorbed by the negative hydrogen.

Significantly more complicated calculations can be carried out for the chromosphere taking into account the non-LTE conditions, and determine its temperature structure.

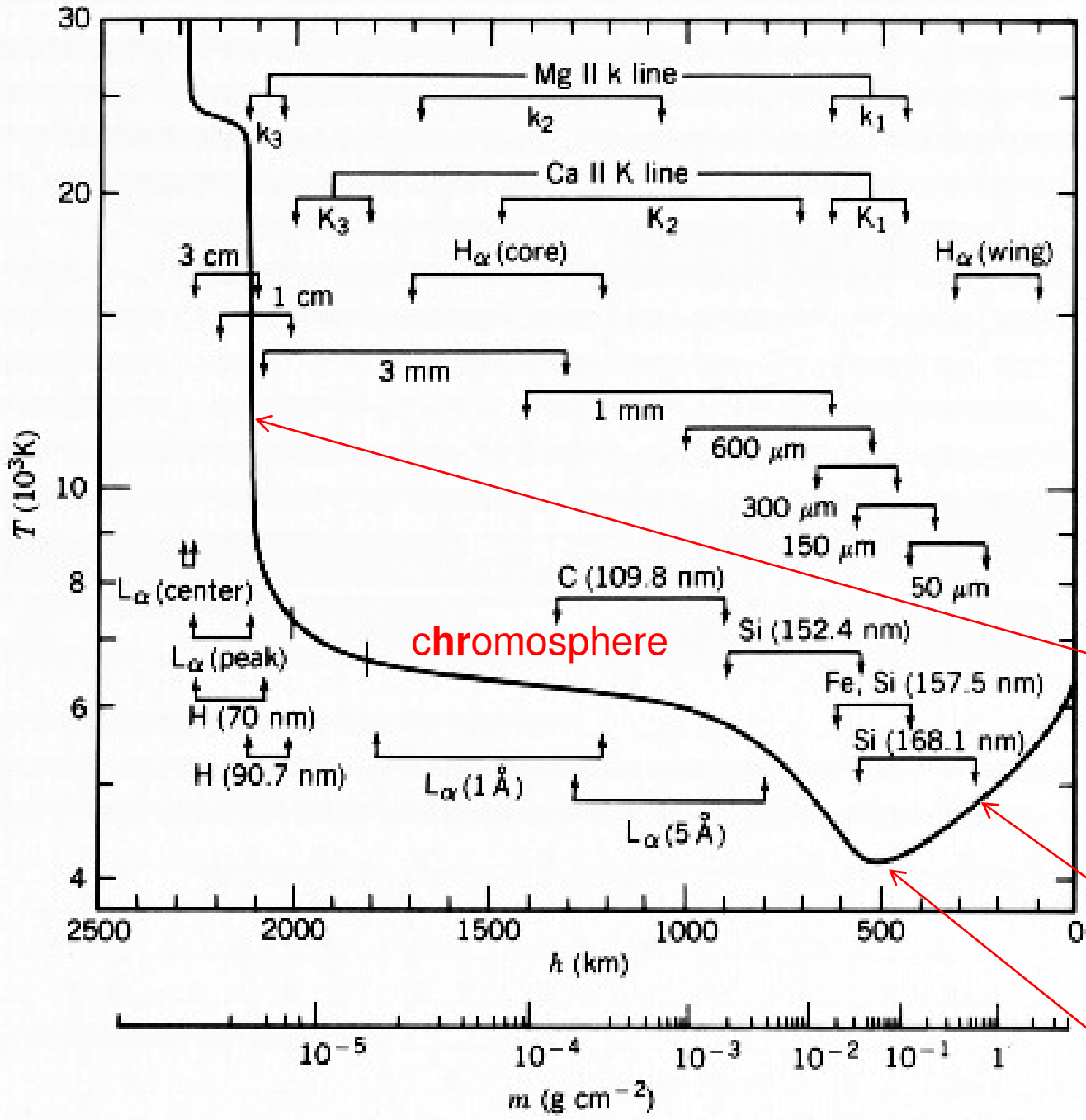

Vernazza, Avrett, Loeser (1981) model of the solar atmosphere (VAL model) showing the approximate regions of formation of various chromospheric radiations.

chromosphere-corona transition region

photosphere

temperature minimum

Filaments and Prominencies

Filaments and prominences are supported by magnetic forces. The simplest model is a magnetic arc the top of which is loaded with a cool heavy gas. Then magnetic field lines should be concaved. The mass of prominences is comparable with the mass of the solar corona. They cannot be formed from condensations of coronal gas.

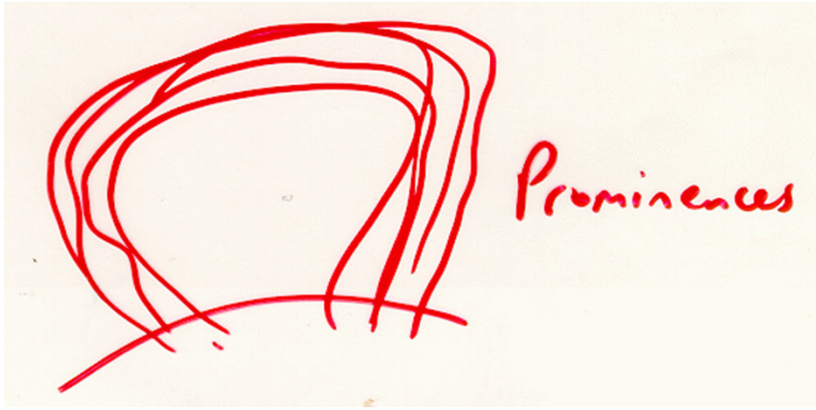

Formation of prominences

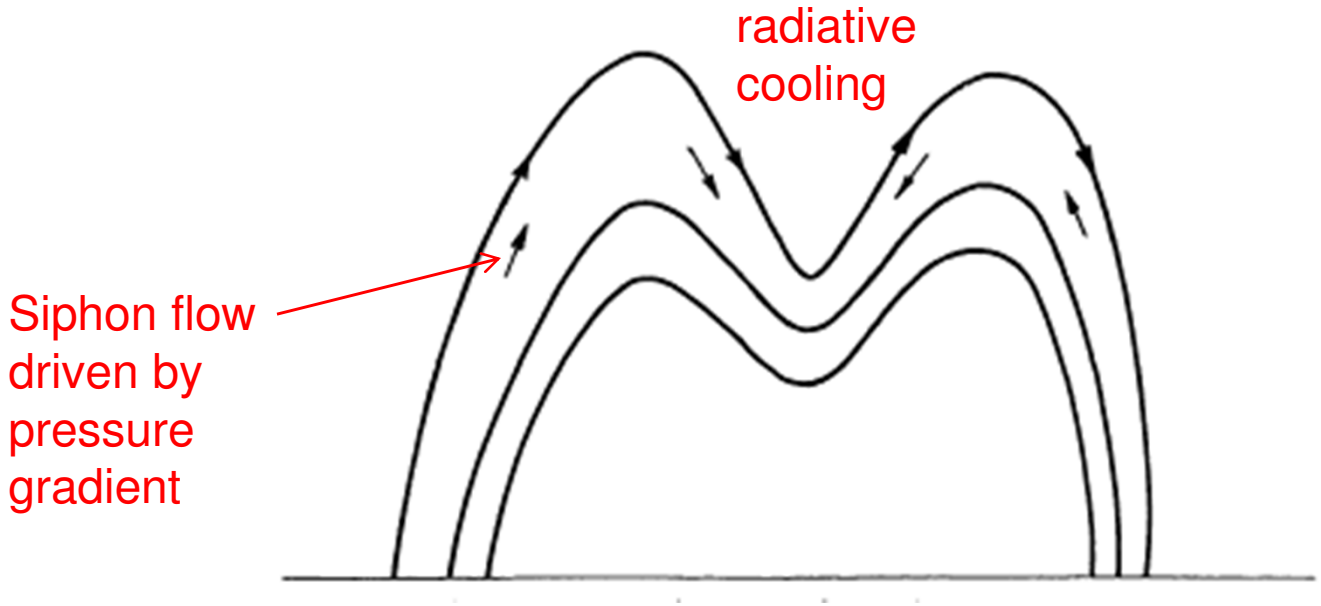

Pikelner (1971) suggested that solar prominences are formed due to evaporation of plasma of low atmosphere. The evaporation flow is driven by a pressure gradient inside the magnetic loop. If one side of a loop is cooler than than the other side, then the pressure gradient drives material to the cooler side. The dense prominence plasma cools because the radiative losses increase with density as ρ^2, and the heating source remains the same. Thus, the prominences are cool because of the loss of the thermal balance.

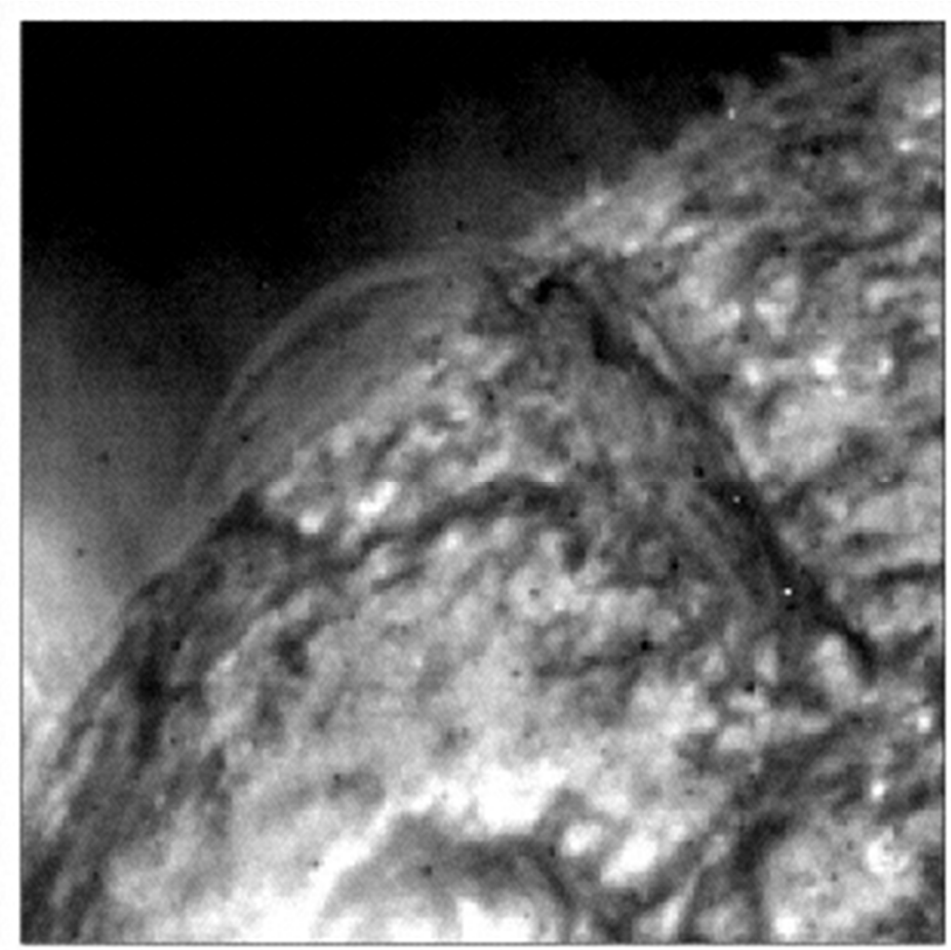

Limbward extension of the He II 304 filament, as seen on 1998 December 14 at 13:19 UT.

Further investigations indicated that the siphon flow may be insufficient for creating prominences of large mass, 10^{16} g. It is suggested that the plasma evaporation is driven by magnetic reconnections in "barbs" located on both sides of the filaments. Analysis of MDI magnetograms and HeII UV data from EIT by Y.-M. Wang ("On the Relationship between He II λ 304 Prominences and the Photospheric Magnetic Field", 2001, Astrophys. J., v.560, 456) provides evidence for magnetic flux cancelation in "barbs".

Filament Observations

Obtained at the Swedish Vacuum Solar Telescope, La Palma, using the Lockheed Tunable Filter in Hα (1998, June 21):

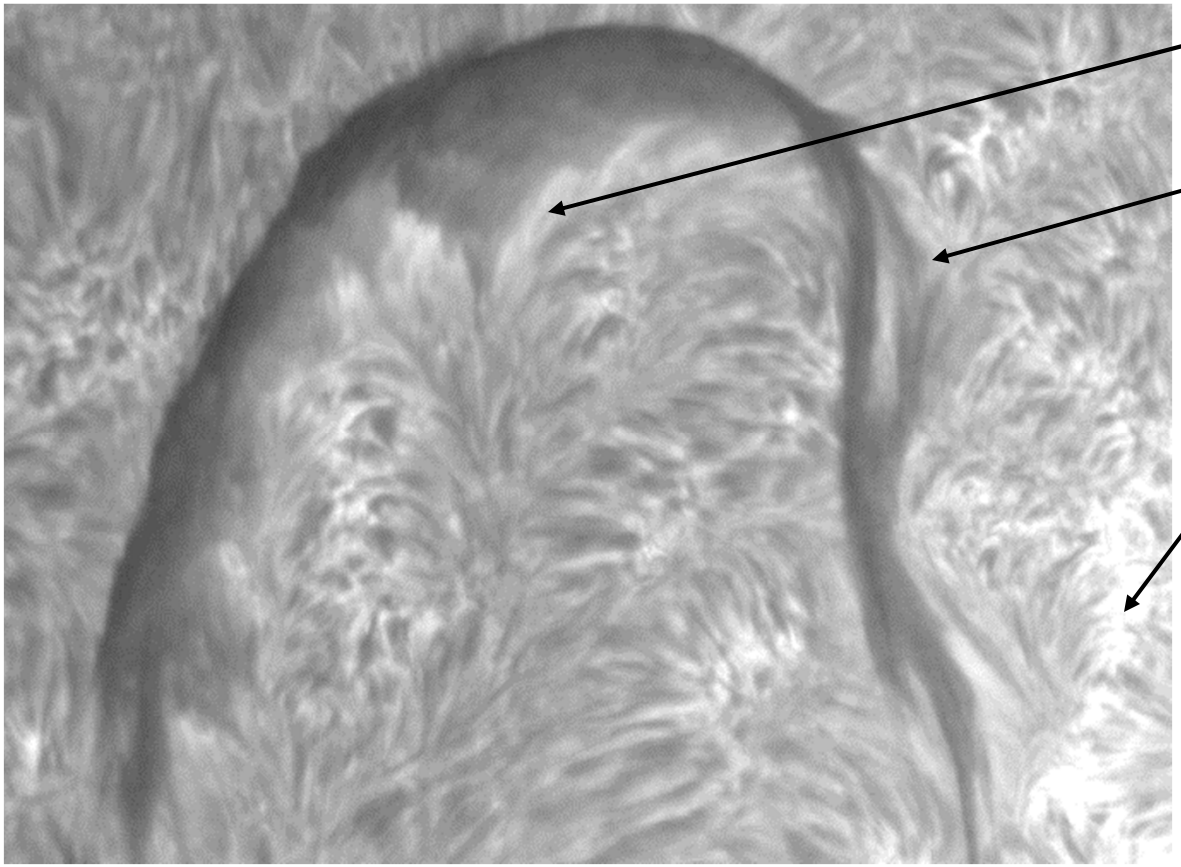

Filament Observations

Dopplergrams based on off-band Hα images (±0.3 Å) show threads within filament:

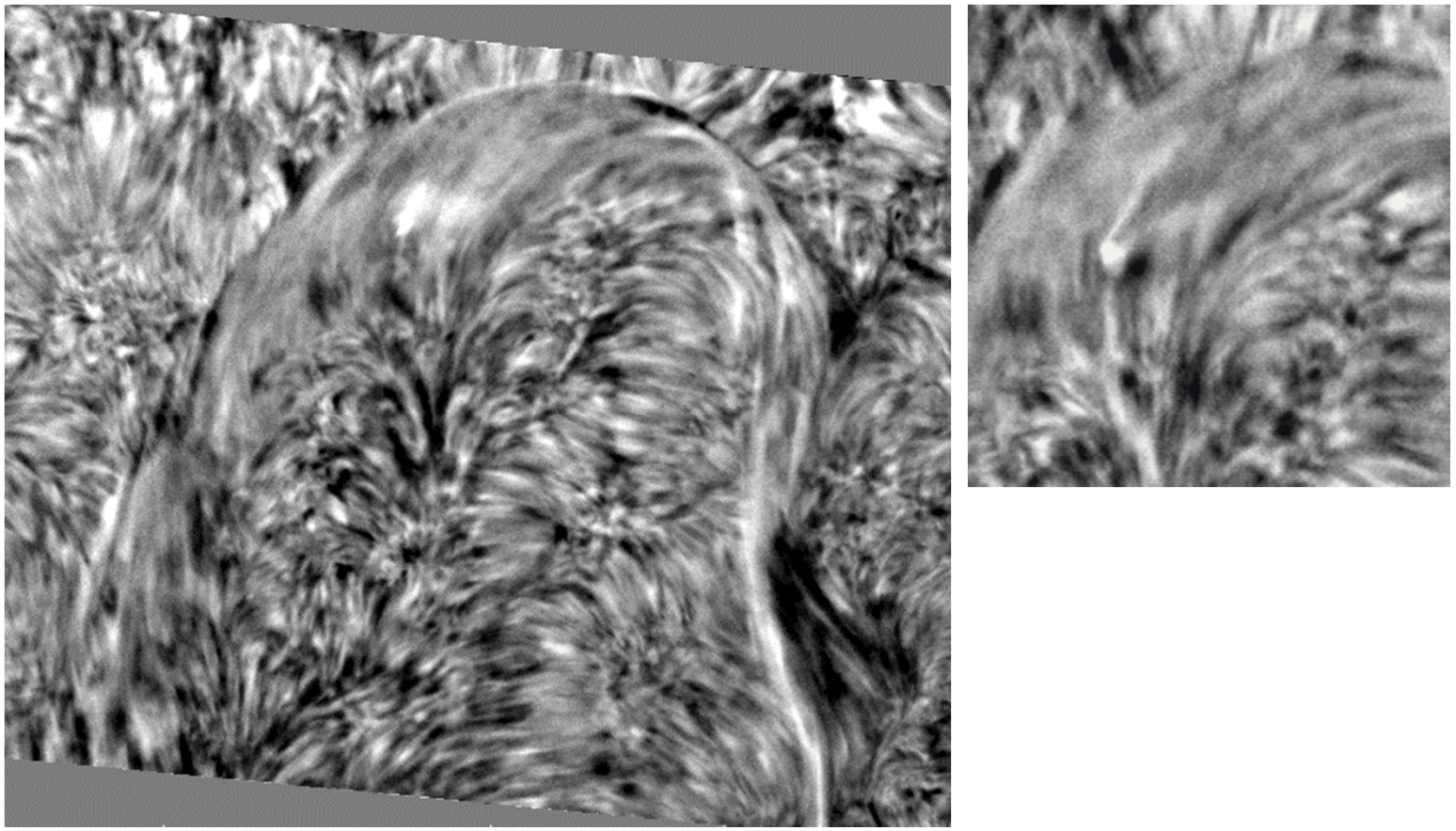

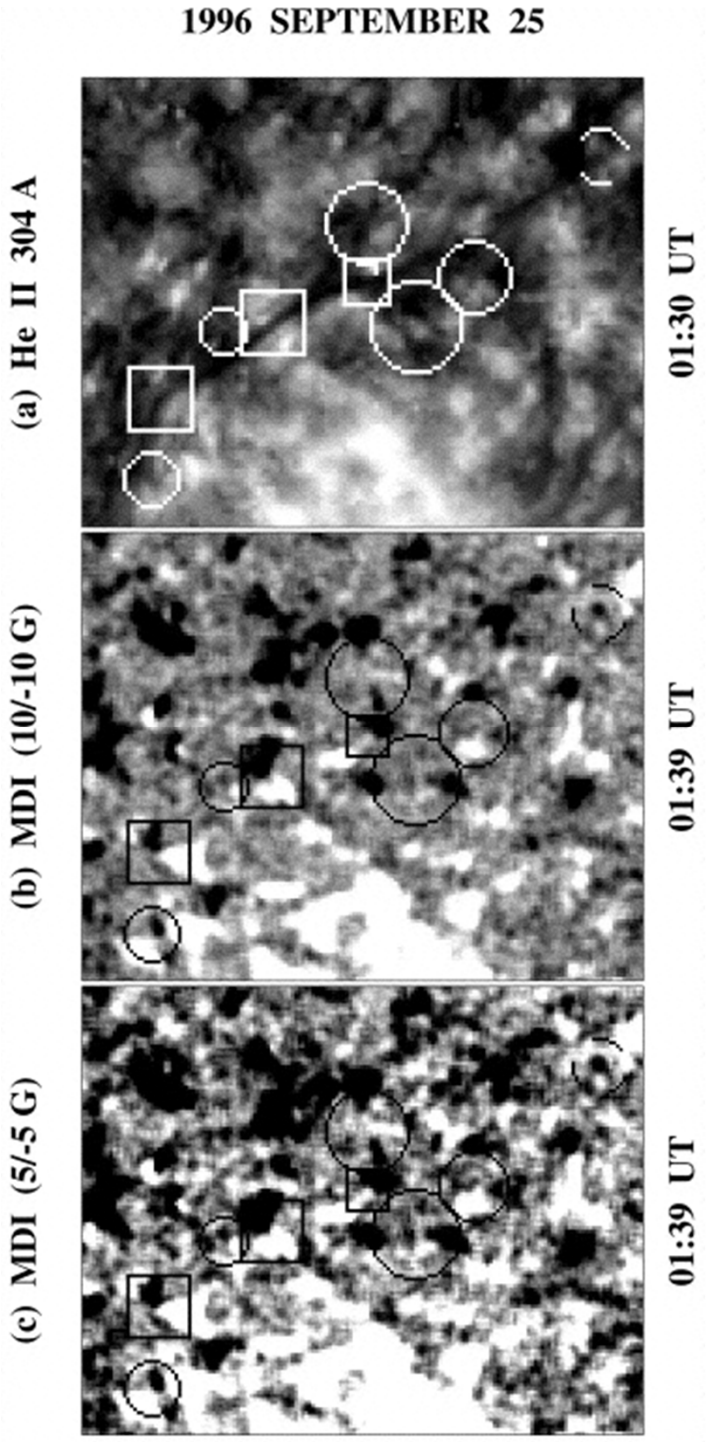

Comparison of a quiescent filament with the underlying photospheric field, 1996 September 25. Here and in subsequent figures, solar north is up and west is to the right.

(a) He II 304 image recorded at 01:30 UT with SOHO/EIT. The dark filament extends diagonally across the field of view, which is centered just below the solar equator.

(b) Line-of-sight magnetogram recorded at 01:39 UT with SOHO/MDI. The field of view coincides with that of the He II 304 image above.

(c) Same as (b), except that the gray-scale levels have been adjusted to reveal weaker fields ranging between -5 G (black) and +5 G (white). The regions of flux cancelations are marked by squares.

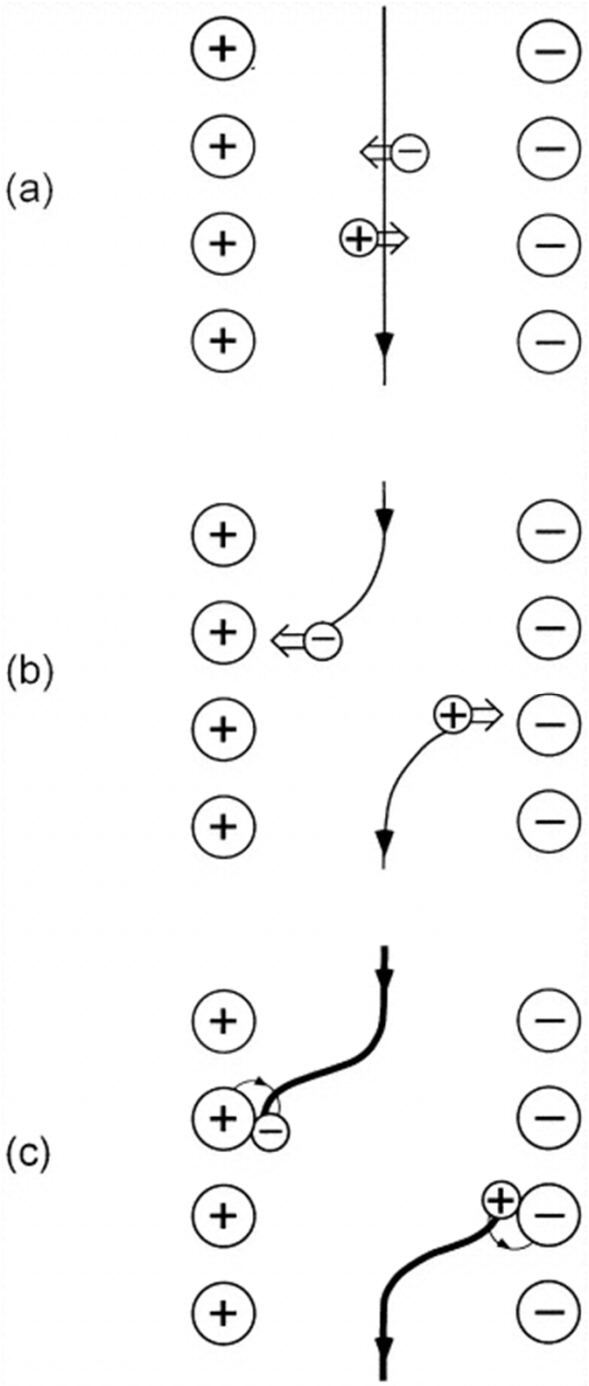

Diffusive mechanism for barb formation. (a) Positive-polarity flux elements diffuse (random walk) from the + side of the filament channel toward the - side, while negative-polarity flux elements diffuse in the opposite direction. The arrowed line represents a southward-pointing axial magnetic field.

(b) As the migrating flux elements cross the filament axis, they become connected to the axial field.

(c) Barbs (thick lines) form when the connected flux elements collide and cancel with the opposite-polarity network fields bordering the filament channel. Note that reversing the direction of the axial field from southward to northward would have produced left-bearing instead of (as here) right-bearing barb

The filaments and prominences are usually located along neutral line of the line-of-sight magnetic field. However, there is a strong transverse component of the field perpendicular to the neutral line. Also, there is evidence that the direction of the transverse field in the corona is opposite to the direction of the photospheric field. That means that the magnetic field in prominences has a helical structure.

DeVore and Antiochos (2000, Dynamical Formation and Stability of Helical Prominence Magnetic Fields, The Astrophysical Journal, 539:954-963) numerically simulated an initially bipolar magnetic field subjected to shear motions concentrated near and parallel to the photospheric polarity inversion line in order to explain the helical structure.

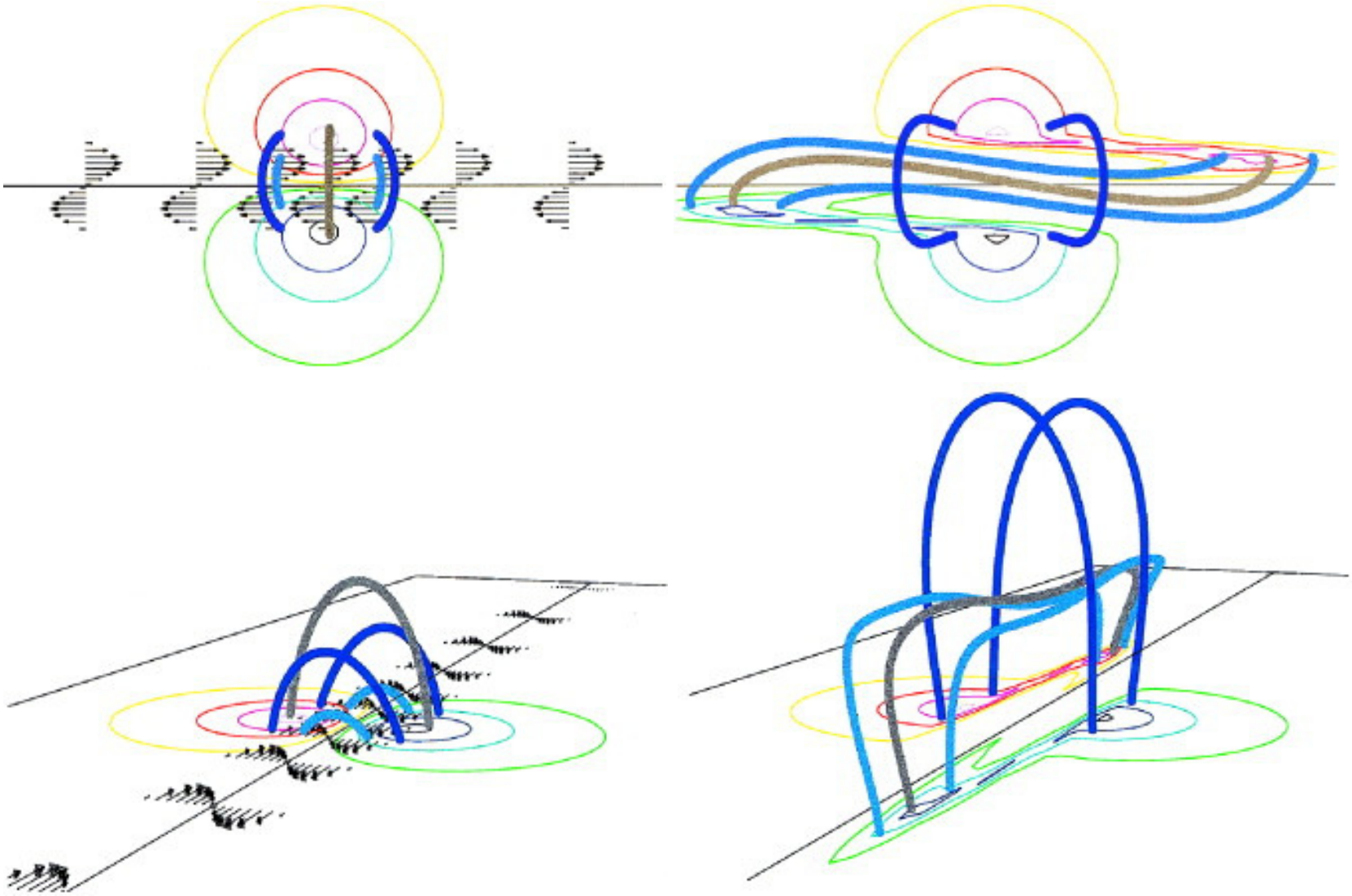

Overhead (upper panels) and perspective (lower panels) views of the initial conditions (left panels) and final results for modest footpoint displacements (right panels) of the prominence model are shown. Color contours on the bottom surface denote lines of constant B_z, while the thick loops denote selected magnetic field lines. The black arrows in the left panels show the direction and relative magnitudes of the imposed footpoint displacements.

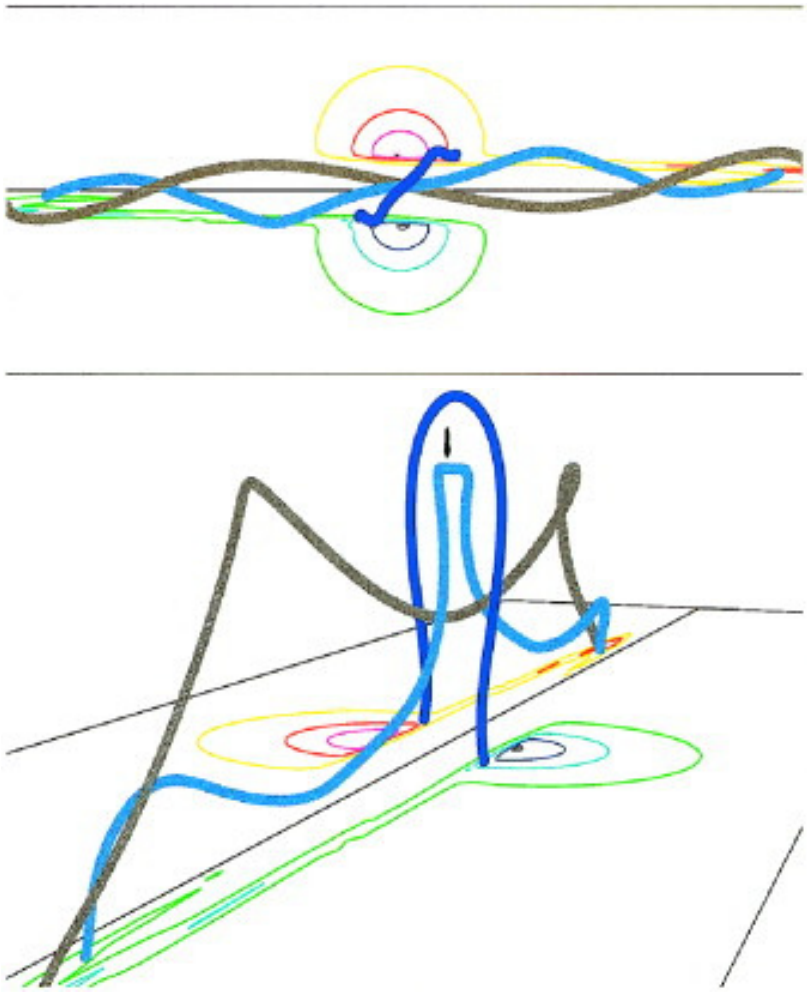

Views of another two groups of field lines, at time $t = 75$ in the simulation before the magnetic lines start reconnecting.

3D modeling of prominences

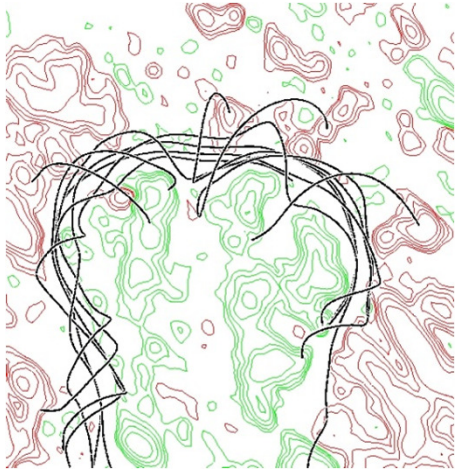

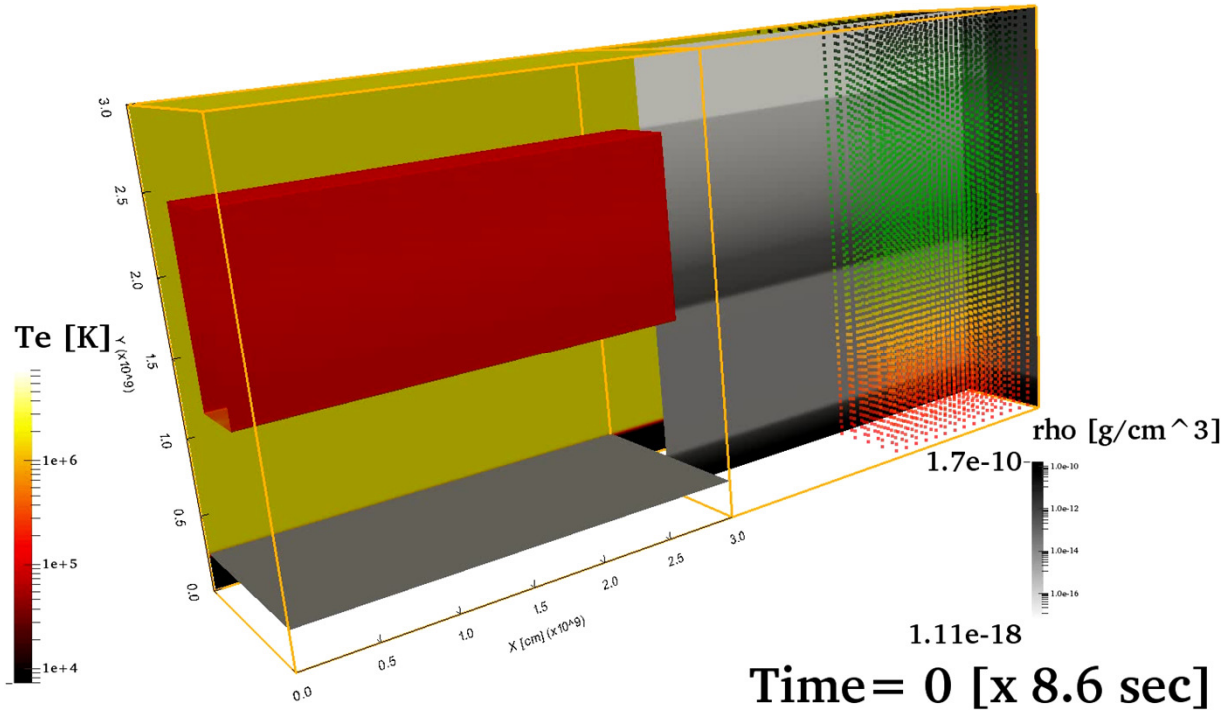

Observations revealed rich dynamics within prominences, the cool (10000K), macroscopic (sizes of order 100Mm) “clouds” in the million degree solar corona. Even quiescent prominences are continuously perturbed by hot, rising bubbles. Since prominence matter is hundredfold denser than coronal plasma, this bubbling is related to Rayleigh–Taylor instabilities. The movie shows true macroscopic simulations well into this bubbling phase, adopting an MHD description from chromospheric layers up to 30Mm height. Our virtual prominences rapidly establish fully nonlinear (magneto)convective motions where hot bubbles interplay with falling pillars, with dynamical details including upwelling pillars forming within bubbles. The simulations show impacting Rayleigh–Taylor fingers reflecting on transition region plasma, ensuring that cool, dense chromospheric material gets mixed with prominence matter up to very large heights. This offers an explanation for the return mass cycle mystery for prominence material. Synthetic views at extreme ultraviolet wavelengths show remarkable agreement with observations, with clear indications of shear-flow induced fragmentations.

(Keppens et al 2015)

Chromosperic Structures

Photoheliogram in the wing of the H_{α} line, of an active region and network near the solar limb. Arrows point to examples of dark mottles.

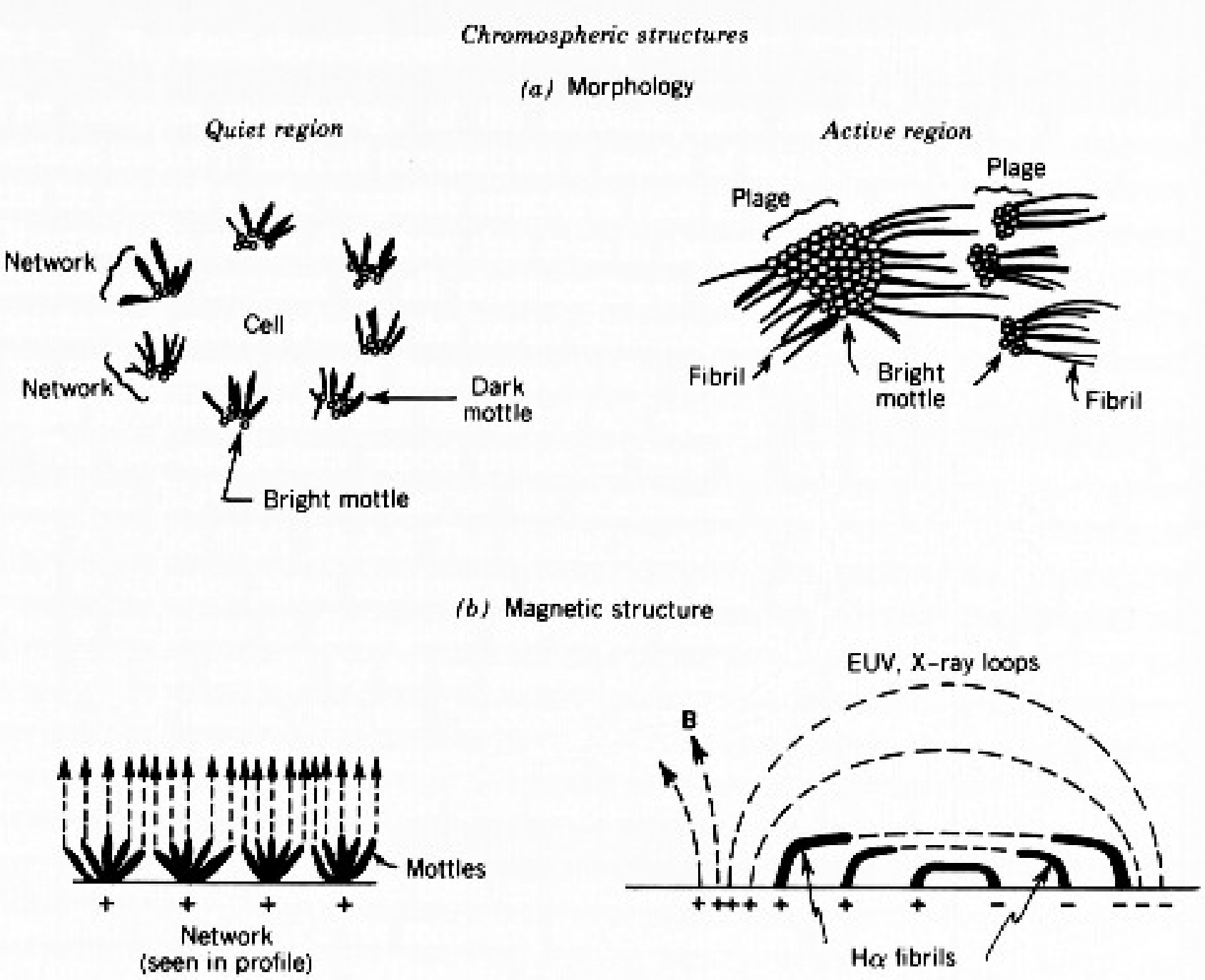
Chromospheric structures
(a) Morphology
Quiet region
Active region
Network
Cell
Network
Dark mottle
Bright mottle
Plage
Plage
Fibril
Bright mottle
Fibril
(b) Magnetic structure
EUV, X-ray loops
B
Mottles
Network (seen in profile)
Hα fibrils

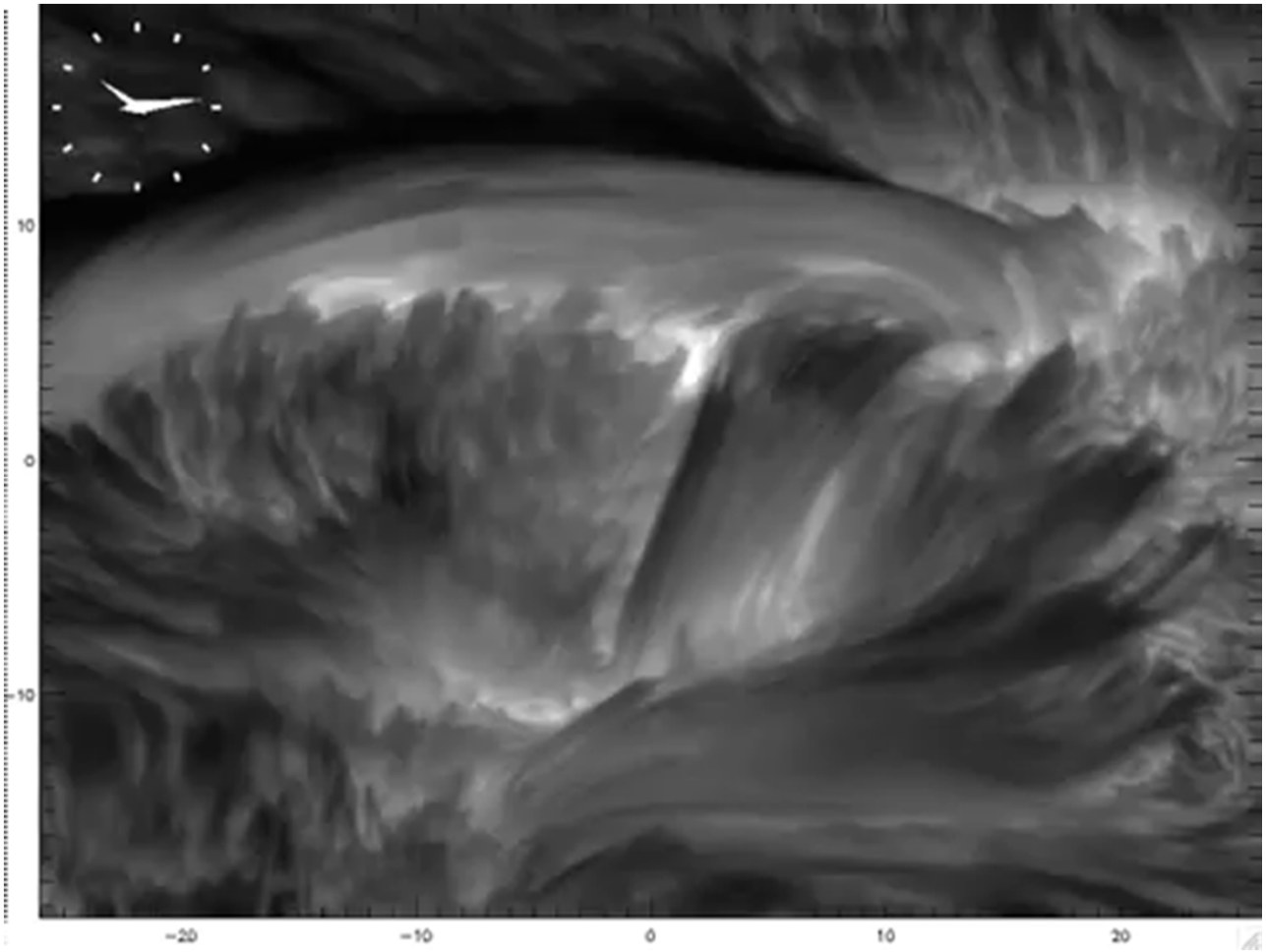

Hα line center imaging from the Swedish Solar Telescope, Courtesy of G. Scharmer, M. Carlsson

Spicule Dynamics

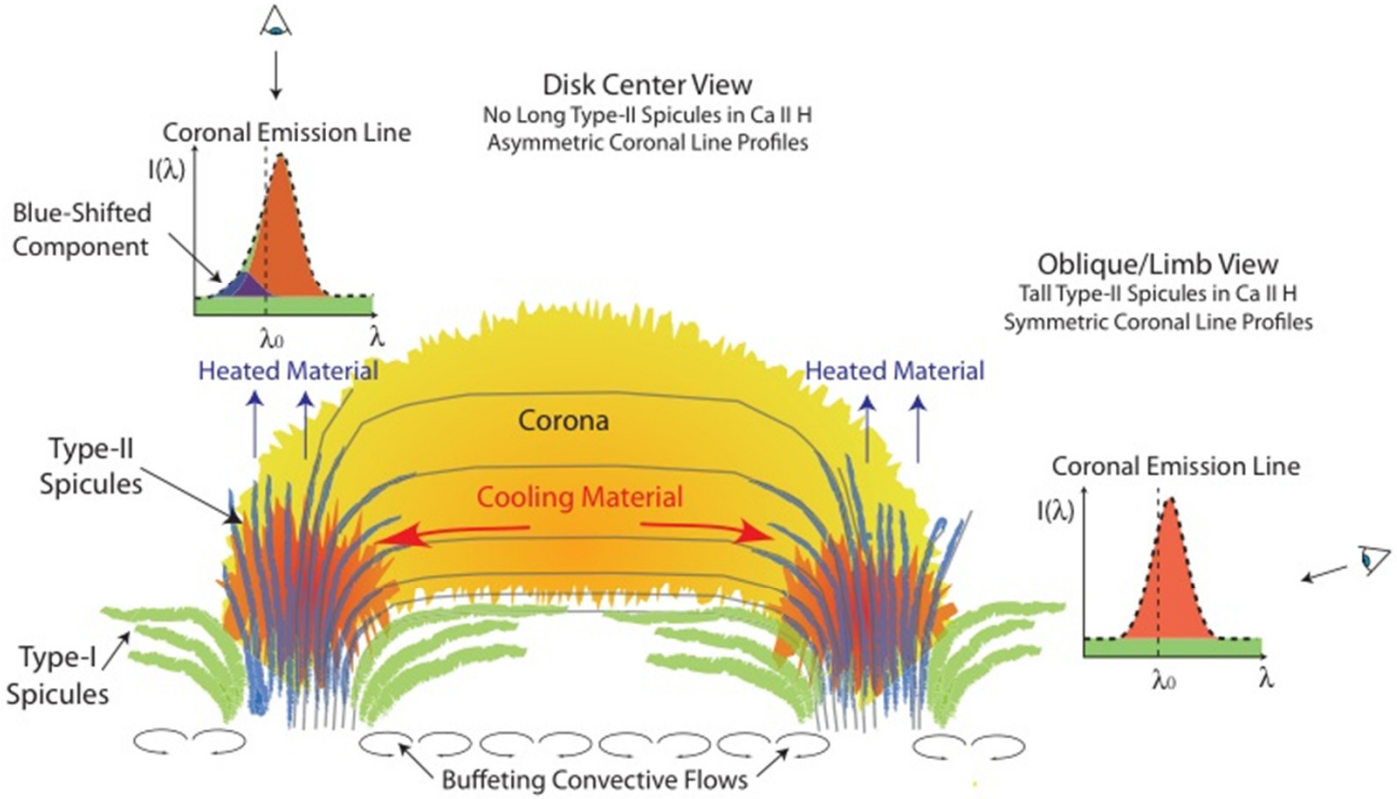

Figure 5. Mass and energy transport between the chromosphere, TR, and corona, as deduced from SOT and EIS observations. See Section 4 for details.

[From De Pontieu, McIntosh, Hansteen, & Schrijver, ApJ 701, L1 (2009)]

Spicules

Consider images of solar spicules obtained on June 18 and 19 of 1997 at at Big Bear Solar Observatory with the 65cm telescope feeding a Zeiss 1/4Å filter and a 1536x1024 Kodak CCD. Overexposed observations were made above the limb as well as normal exposures on the limb. The filter was tuned to Ha -0.65 and a 30 sec 1/4Å interval was used.

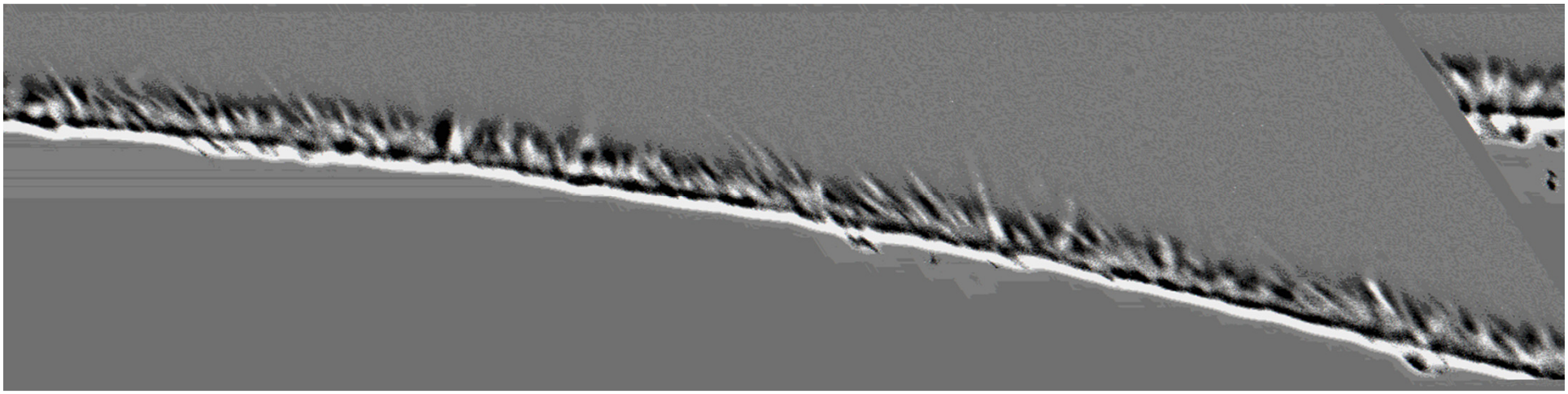

About 200 arc seconds of the north limb of the Sun was observed for 5 hours on June 19. Observations were made of the equatorial limb as well for comparison, but this took place after the 5 hours of good seeing and is not strictly comparable. Events on the limb are mainly moving in the plane of the sky and the fact that observations were made at -0.65Å did not really produce important wavelength shift effects, as the typical spicule profile is more than 1Å wide. Figure shows one of the best images; the dark band along the limb results from the spatial filtering. Rather than the commonly expected up-and-down motion, the spicules tended to fade, sometimes quite abruptly, when they reached the top of their trajectory. This is quite evident when one views the observations in movies running back and forth. In the backward movies, no upward surging is seen, which means that there is no rapid sinking to the surface reversing the upward path.

(Zirin & Cameron, 1997)

The lifetimes of most of the events were fairly short, certainly no longer than 10 minutes and some only visible for a few minutes. The figure shows a normal background of smaller spicules about 4,000 or 5,000 kilometers high above the limb. The higher events, which extend as high as 20,000 kilometers above the surface, were observed in a whole variety of forms and a wide range of brightness.

First there are long spicules, which were observed both vertical and tilted as far as 30 degrees from the radial. While these had the classic shape we tend to think of, very few if any were seen to return to the surface. In general, they would extend and then fade out at the top of their trajectory. In some cases these are multiple.

The second class was eruptions, which fly up to about 15,000 kilometers in an irregular way. The velocities inferred from the proper motion of these events are quite large, between 50 and 100 km/sec.

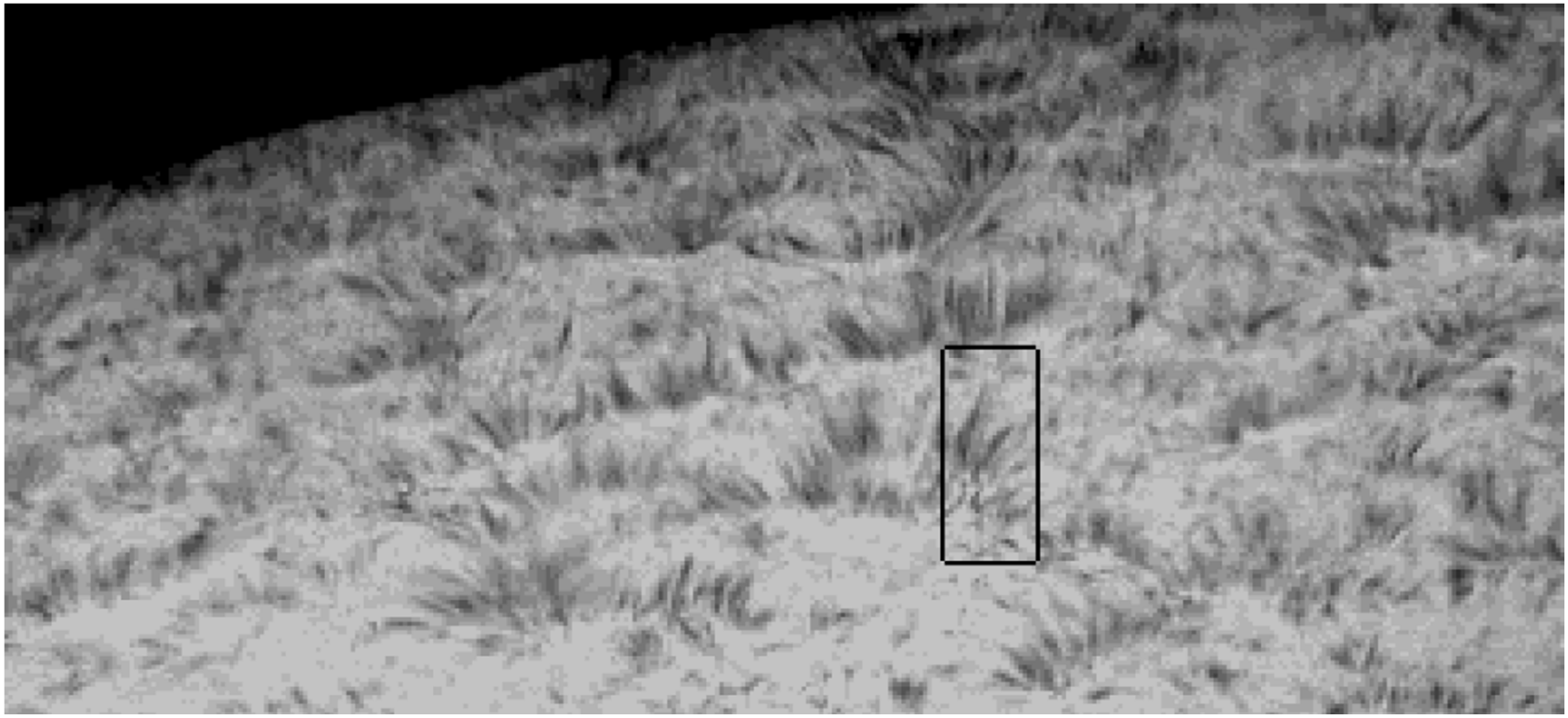

The appearance of the spicules on the disk is shown, a frame at Ha-0.65Å, which has been somewhat sharpened. The spicules appear slightly different from those at the limb, mostly because the bases are visible. Long spicules, which likely correspond to macrospicules, were easily visible, and arose in the same bushes as normal spicules.

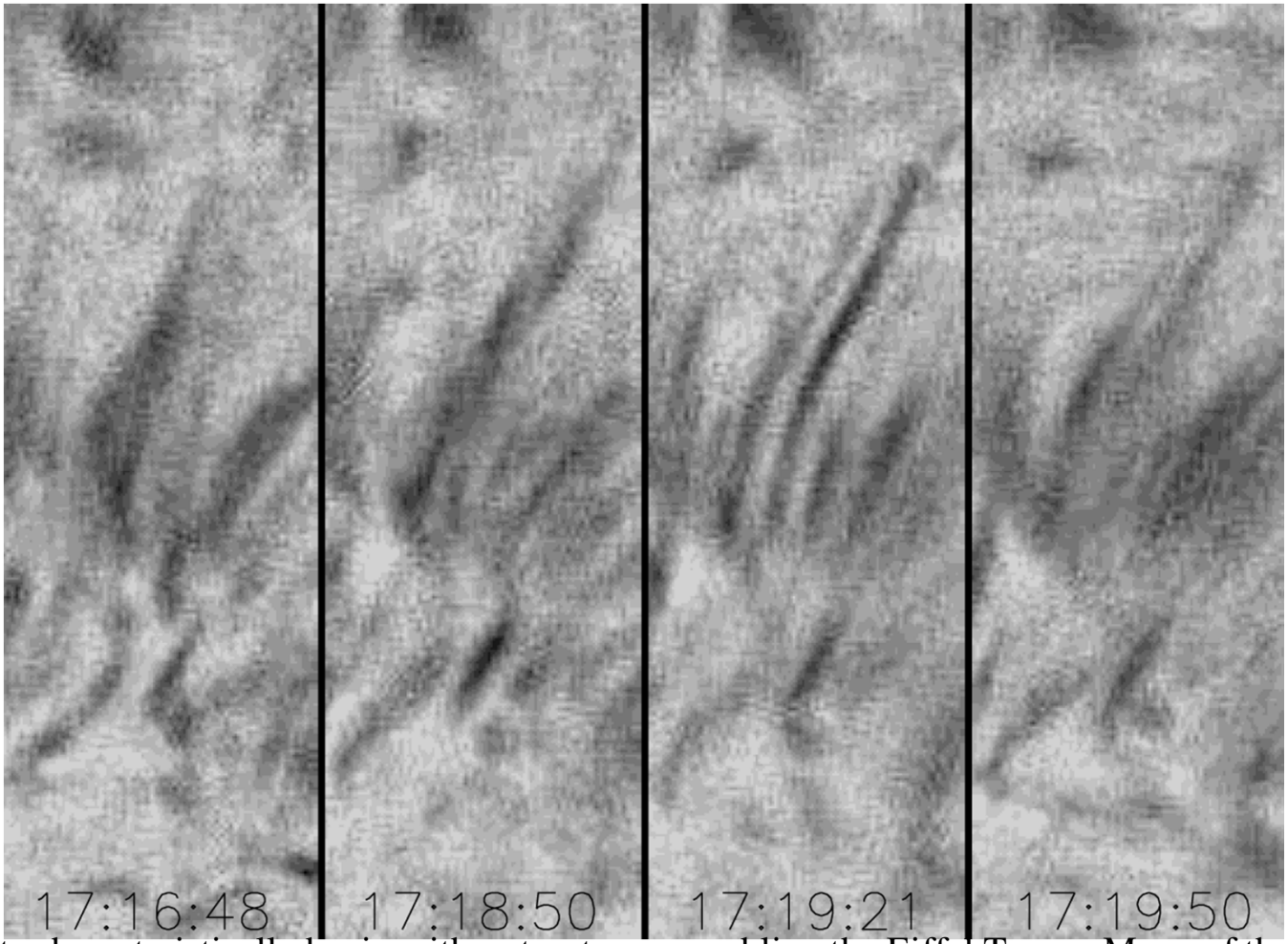

Macro events characteristically begin with a structure resembling the Eiffel Tower. Many of these features were seen, at least two or three at any given time. They rise to a height of about 15,000 kilometers and then appear to twin into a double spicule and fade away. Beside the Eiffel Tower form, simple macrospicules appear, unstructured elongated single or multiple forms. These various forms are seen on images which mostly have single spicules. In Figure, one sees clearly how the Eiffel Tower structure evolves into what may be a rotating or twisting spicule and then into a twin spicule. The twin spicule fades away fairly quickly, not lasting more than one minute. The whole process takes less than 4 minutes.

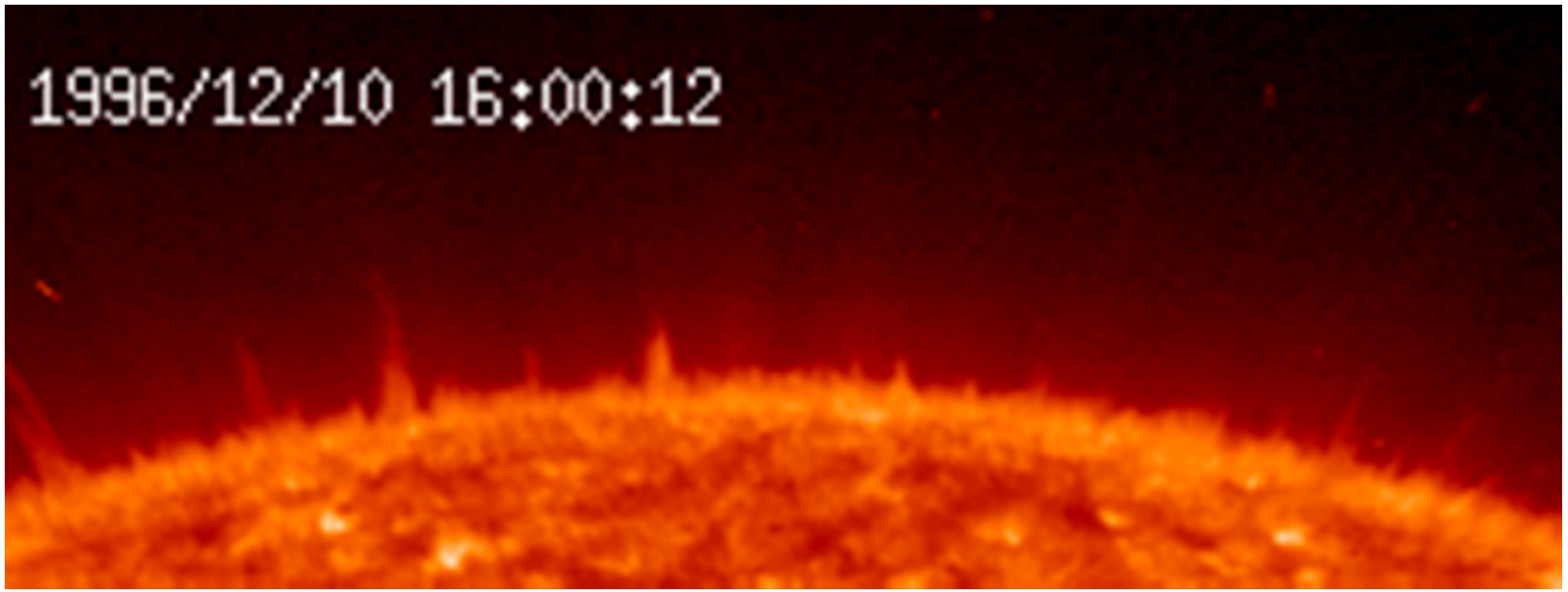

He II 284A

Kudoh and Shibata (1999, "Alfven Wave Model of Spicules and Coronal Heating", The Astrophysical Journal, Volume 514, Issue 1, pp. 493-505) performed MHD simulations for torsional Alfven waves propagating along an open magnetic flux tube in the solar atmosphere. It is shown that, if the root mean square of the perturbation is greater than 1 km s^{-1} in the photosphere, the transition region is lifted up to more than 5000 km (i.e., the spicule is produced).

They assumed that the Alfven waves are generated by random motions in the photosphere. As the Alfven waves propagate upward in the solar atmosphere, longitudinal motions are excited by the nonlinear couplings. The longitudinal motions propagate upward as slow or fast waves and lift up the transition region (i.e., the spicule is produced). A part of the Alfven waves are reflected in the transition region, but the remaining waves propagate upward to the corona and contribute both to the heating of the corona and the nonthermal broadening of emission lines. The result of their simulation would suggest that the quiet hot corona, nonthermal broadening of lines, and spicules are caused by Alfven waves that are generated in the photosphere.

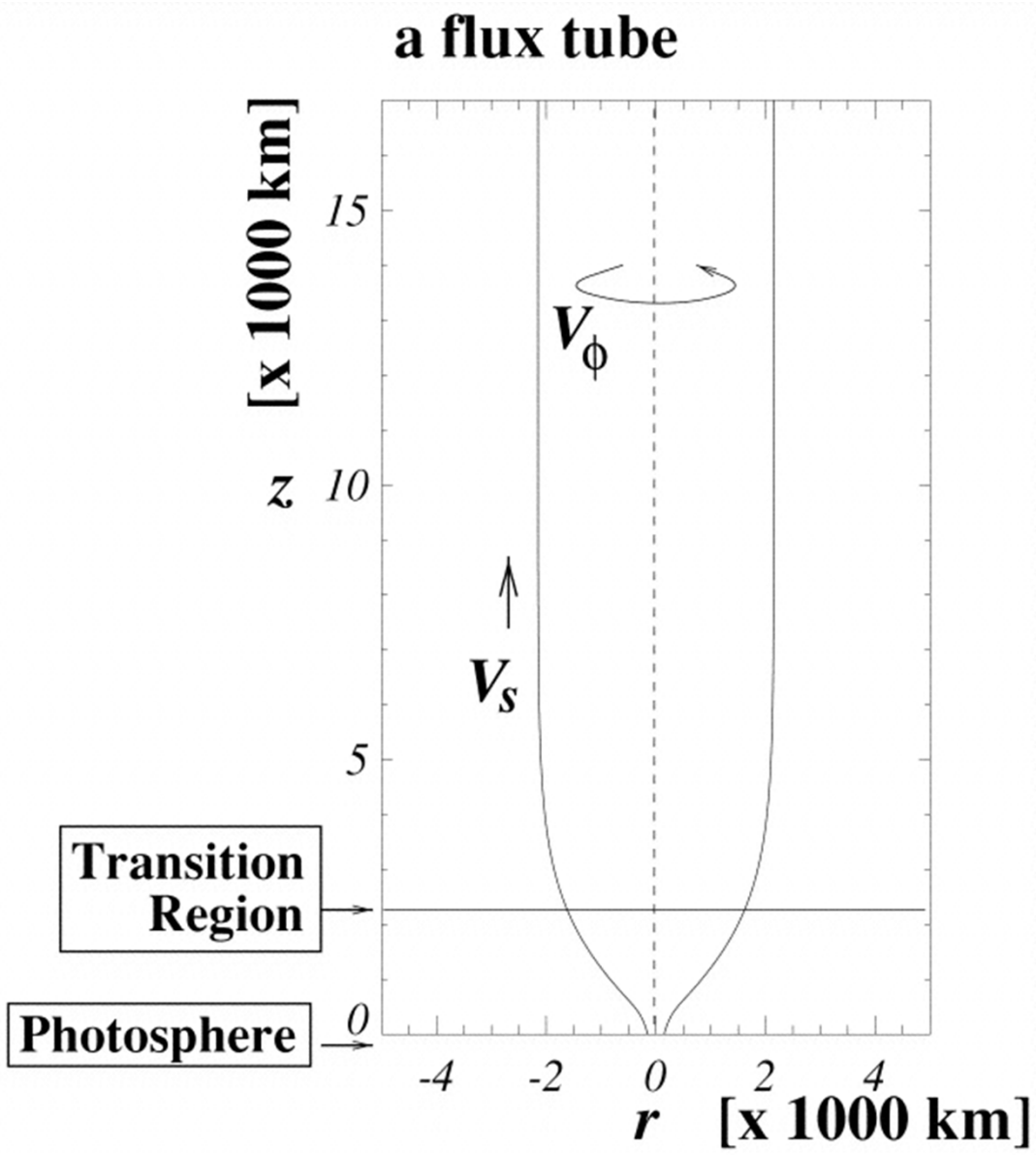

Shape of the model flux tube. The transition region is initially z=2250 km from the photosphere.

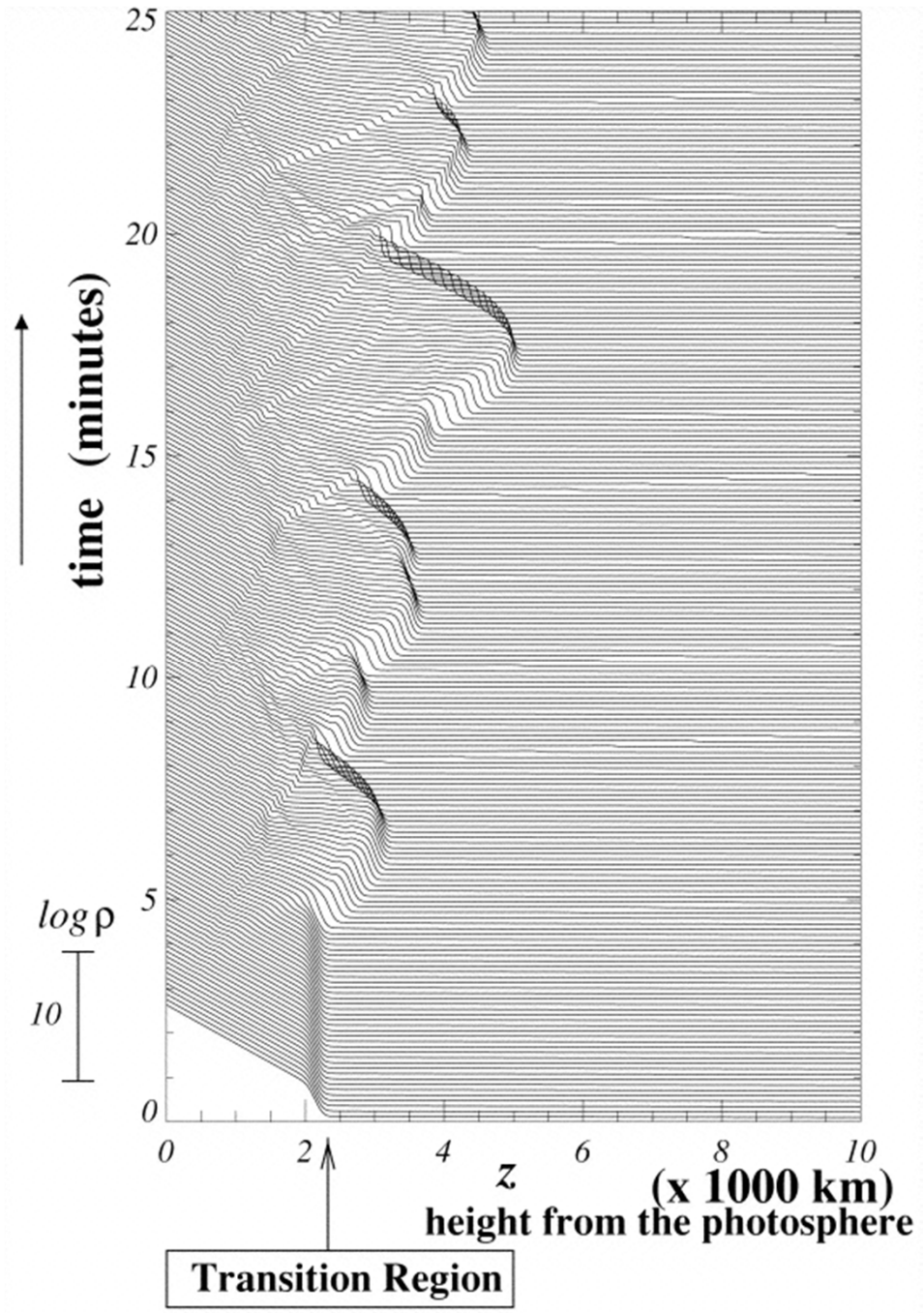

Time variation of density distribution. The plots at various time are stacked with time increasing upward in uniform increments of 7.2 s.

Observation of atmospheric dynamics from Hinode

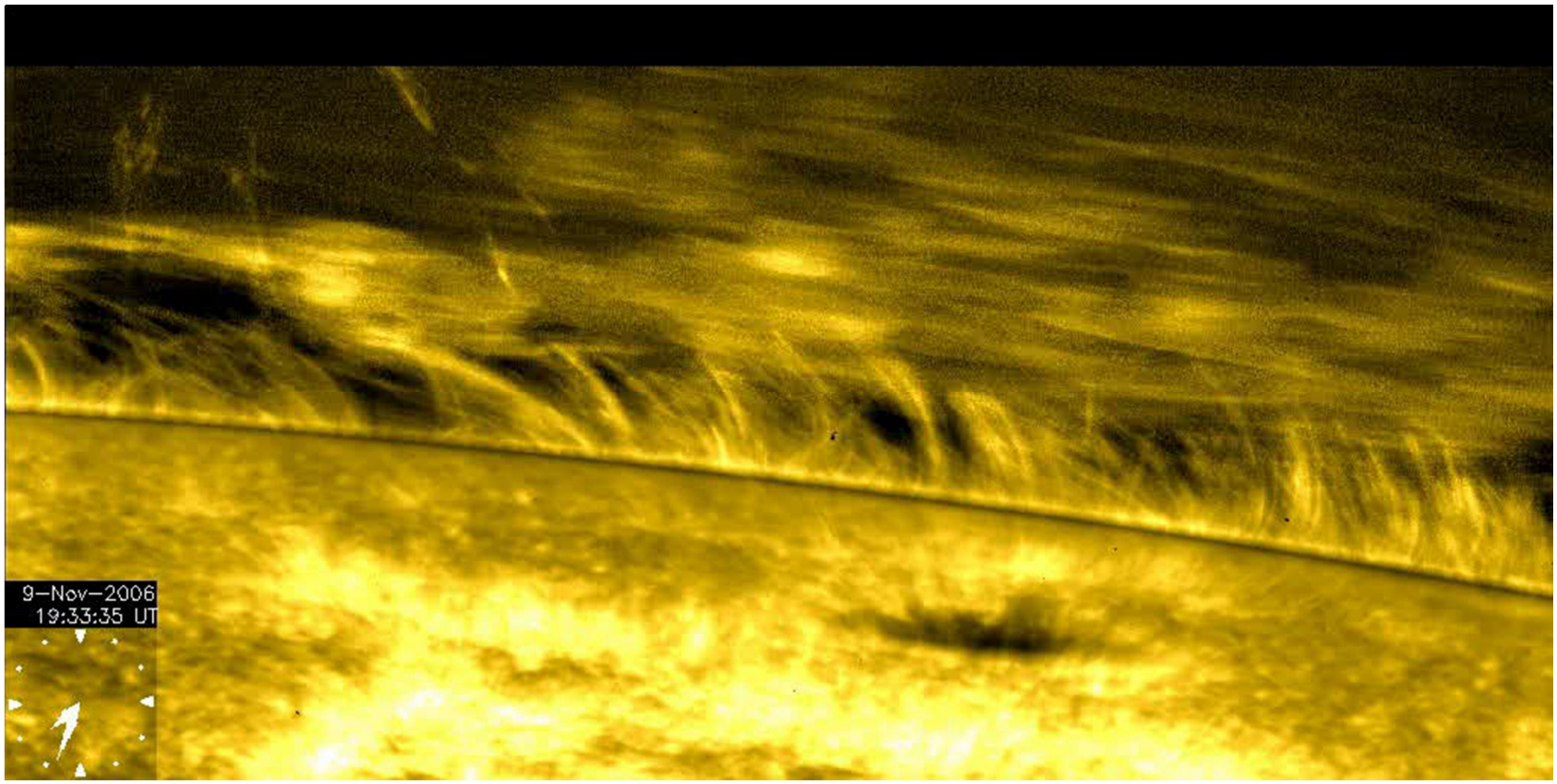

It was found that most spicules show up double thread structure during their evolution. This feature was already mentioned by Tanaka for disk mottles in high resolution H-alpha wing observation (1974) . Therefore it is likely that the spicule and disk mottles in quiet Sun have the same origin. New findings for the spicules are that the separation of the double threads change with time by the spinning as a whole body; repeating phases single and double threads.

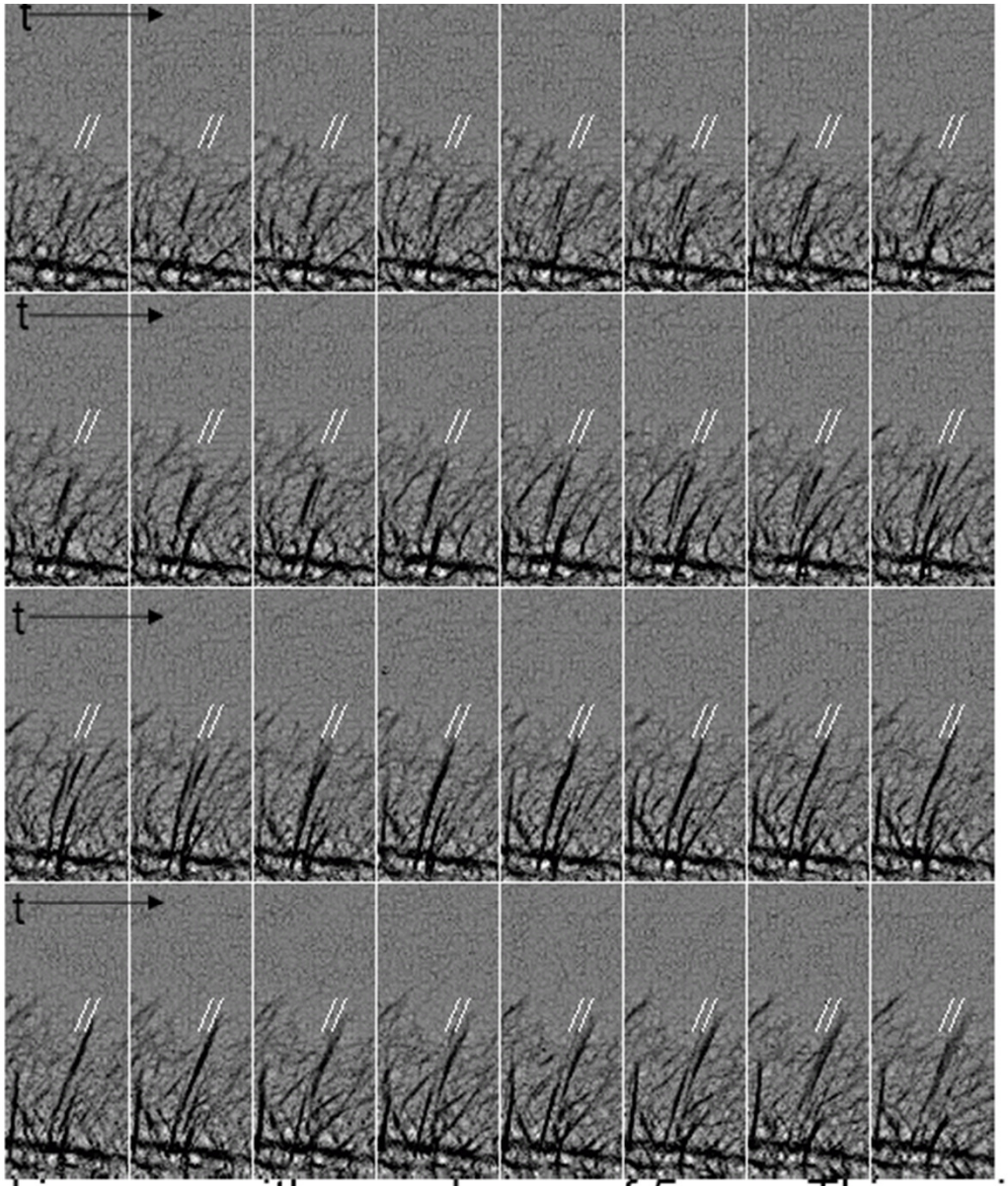

Sharpened images with a cadence of 5 sec. This series clearly show that the spicule of double threads (indicated by white lines) is spinning as a whole body (spin period: 1 - 1.5 min, v∼15 km/sec).

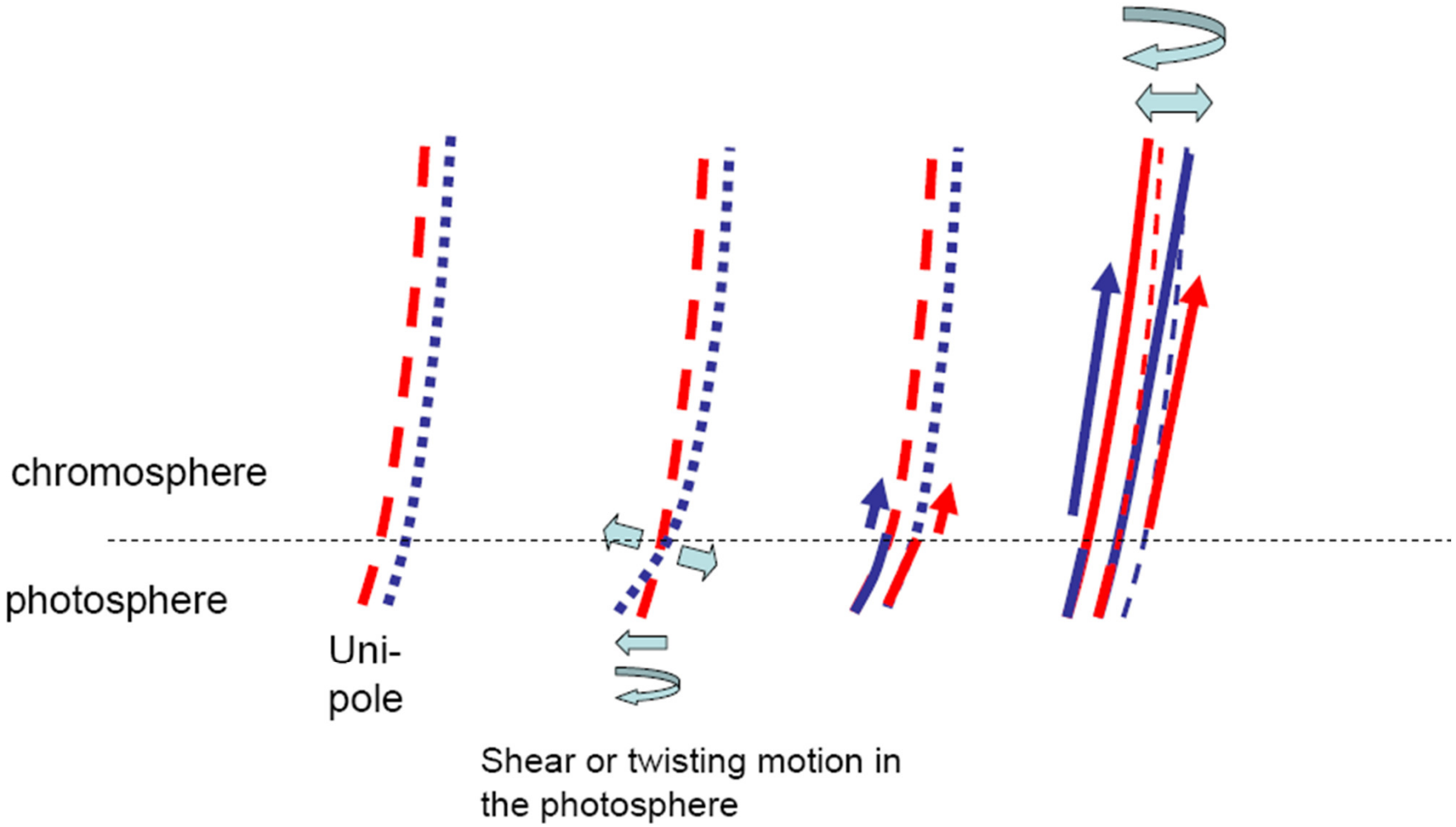

Speculative magnetic reconnection model to explain the double thread structure of spicule and following evolution (expansion thread separation, lateral motion and spinning as a whole body).

Hinode observations provided evidence of two types of spicules

- "Type-I" spicules – material returns to the surface. They are possibly driven by shock waves that form when global oscillations and convective flows leak into the upper atmosphere along magnetic field lines on 3–7 minute timescales.
- "Type-II" spicules do not return - "fade out". They are much more dynamic: they form rapidly (in ~10s), are very thin (≤200 km wide), have lifetimes of 10–150s (at any one height), and seem to be rapidly heated to (at least) transition region temperatures, sending material through the chromosphere at speeds of order 50–150 km s^{-1}.
- The properties of Type II spicules suggest a formation process that is a consequence of magnetic reconnection, typically in the vicinity of magnetic flux concentrations in plage and network.

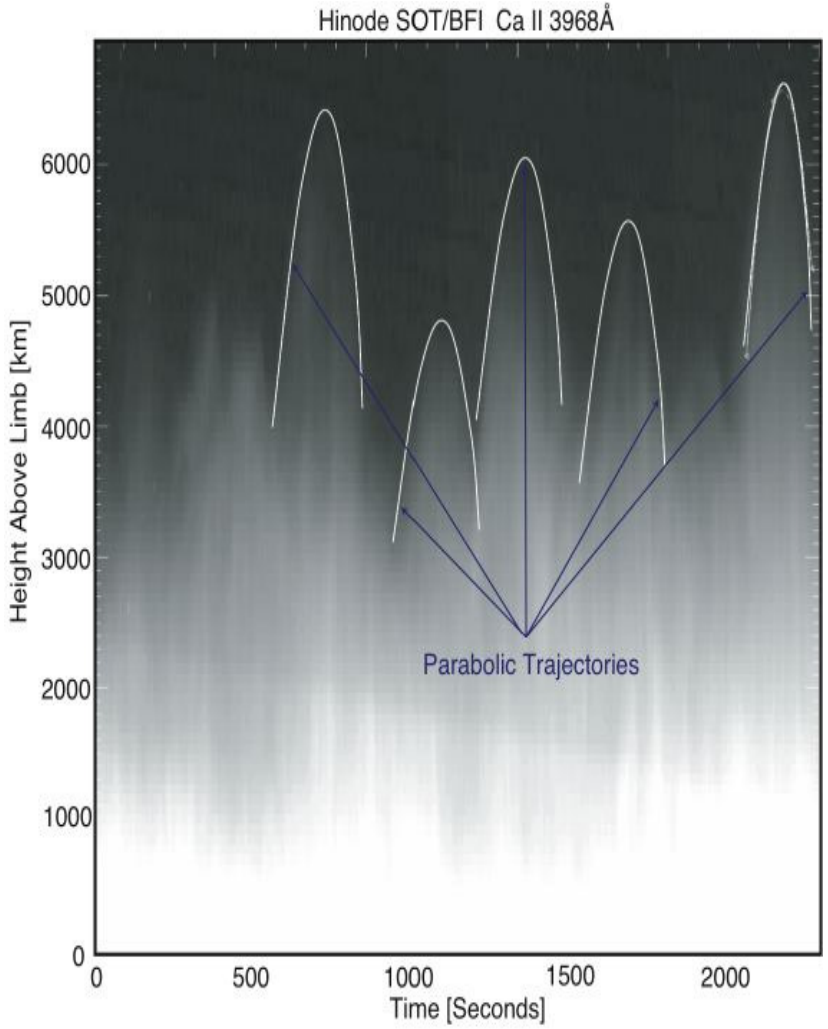

(De Pontieu et al 2007)

The observations of spicules from IRIS (Interface Region Imaging Spectrograph)

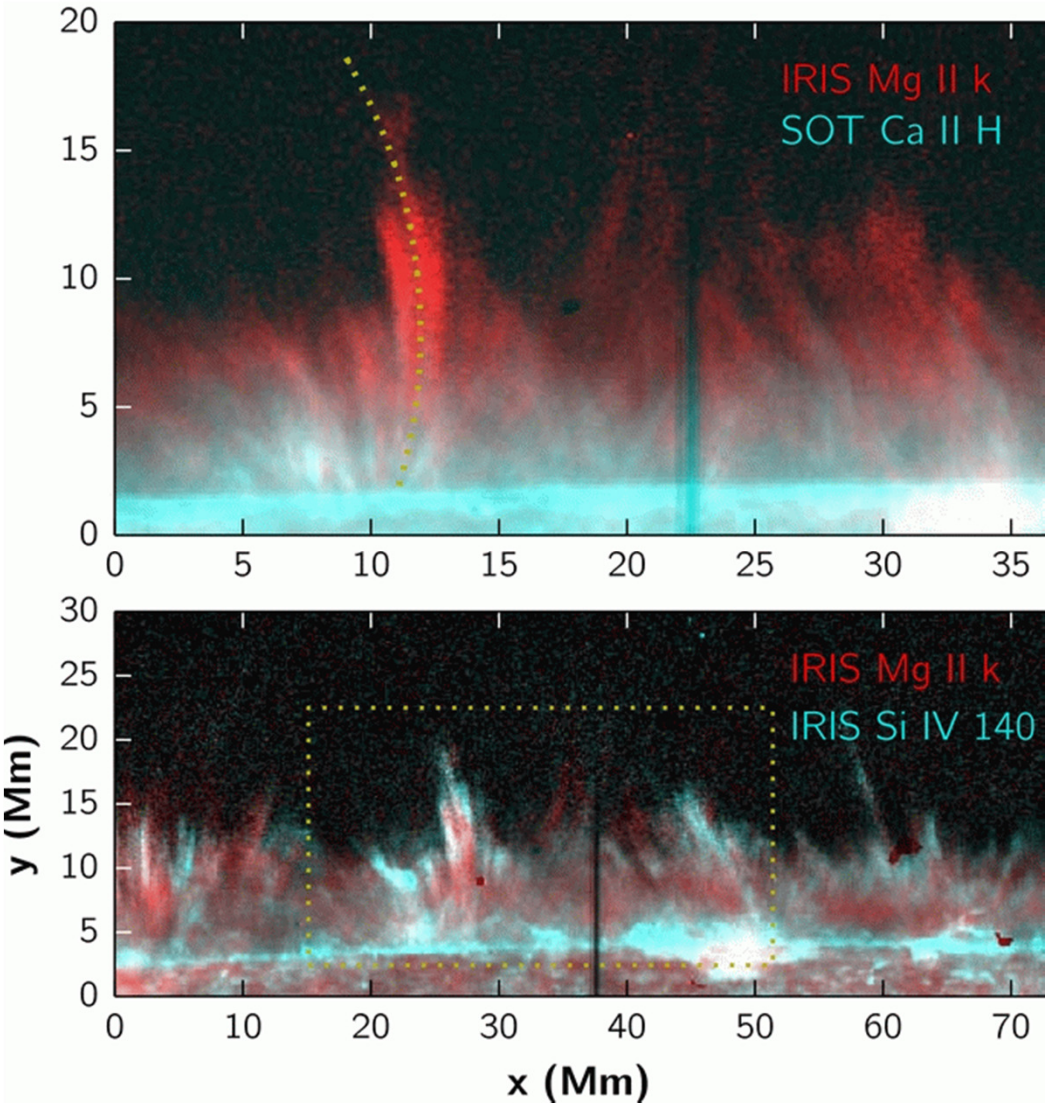

The group behavior of spicules is clearer in the IRIS observations. What is often perceived as one or two spicules in SOT turns out to be a much wider structure in IRIS. With clearly defined multiple strands, these wide bunches of spicules have the same time evolution, and extend to areas with little or no emission in Ca ii. Such group behavior plausibly contributes to the appearance of seemingly co-spatial spicules in lower-resolution observations It is likely that only the cooler strands of such groups become visible in Ca ii. The group behavior, multi-thermal nature, and apparent heating of these spicules indicate that these features are likely not driven in the same way as dynamic fibrils.

(Pereira et al. 2014).